Photoacoustics 23 (2021) 100281

Contents lists available at ScienceDirect

Photoacoustics

journal homepage: www.elsevier.com/locate/pacs

Optothermal properties of plasmonic inorganic nanoparticles for photoacoustic applications

Cristina Gellini, Alessandro Feis *

Dipartimento di Chimica "Ugo Schiff", Università di Firenze, Via della Lastruccia 3, I-50019 Sesto Fiorentino (FI), Italy

ARTICLE INFO

Keywords:
Nanostructured materials
Plasmonic bands
Photothermal properties
Contrast agents
Inorganic nanoparticles

ABSTRACT

Plasmonic systems are becoming a favourable alternative to dye molecules in the generation of photoacoustic signals for spectroscopy and imaging. In particular, inorganic nanoparticles are appealing because of their versatility. In fact, as the shape, size and chemical composition of nanoparticles are directly correlated with their plasmonic properties, the excitation wavelength can be tuned to their plasmon resonance by adjusting such traits. This feature enables an extensive spectral range to be covered. In addition, surface chemical modifications can be performed to provide the nanoparticles with designed functionalities, e.g., selective affinity for specific macromolecules. The efficiency of the conversion of absorbed photon energy into heat, which is the physical basis of the photoacoustic signal, can be accurately determined by photoacoustic methods. This review contrasts studies that evaluate photoconversion in various kinds of nanomaterials by different methods, with the objective of facilitating the researchers' choice of suitable plasmonic nanoparticles for photoacoustic applications.

1. Introduction

The world of photoacoustics is currently being pervaded by innovative materials, among which plasmonic nanoparticles (PNPs) represent one of the main constituents [1–3]. Several aspects make these systems attractive for photoacoustic applications. In particular, plasmonic resonances immediately lead to a strong light / matter interaction. Notably, the absorption cross section of metal nanoparticles is expected to be larger than that of dye molecules by at least one order of magnitude [4]. It is recalled that a high level of light absorption is the basis for effective generation of photoacoustic signals. In addition, plasmonic resonances give a particular versatility to PNPs, as an optimum excitation light wavelength can be selected in relation to the size, shape and composition of the nanoparticle in question. Together with the bulk chemical properties, it is nowadays possible to control the surface chemistry of PNPs. In particular, surface functionalization can be performed producing tailored species that can selectively react with important target molecules [5]. Finally, the generation of photoacoustic signals can be ably exploited for photoacoustic imaging (PAI). This technique can be performed by exciting either the signals of the constituent molecules of living cells, or those of exogenous contrast agents [6,7]. PNPs appear to be especially well suited for PAI because of their optical and optothermal properties [8–10].

Localized surface plasmon resonance (LSPR) is the basis of the interaction between light and PNPs. The theory and experimental approach adopted to explain such phenomena were originally developed for metal PNPs for which the physical size scale is much smaller than the light wavelength used [11–13]. The simplest shape of a nanoparticle – especially for ease of calculation – is that of a sphere. In addition, spheroids can be treated by specifically modified analytical models [14]. More complicated shapes can be theoretically investigated by numerical calculations or analytical methods [15]. The case of anisotropic PNPs is especially interesting, as they display additional degrees of freedom yielding enhanced LSPR versatility [16]. Recent progress in PNP synthesis has allowed PNPs of different morphology to be obtained characterized by high chemical purity and preparation reproducibility. Moreover, the reaction products of modern syntheses can be designed in such a way that the resultant PNPs effectively absorb light within the first (650 nm – 850 nm) or second (950 nm – 1350 nm) near infrared (NIR) window [17]. These wavelength regions are of particular interest for biomedical applications, particularly for those based on photoacoustic approaches. They are named "windows"

Abbreviations: PNP(s), plasmonic nanoparticle(s); PAI, photoacoustic imaging; LSPR, localized surface plasmon resonance; NIR, near infrared; PTT, photothermal therapy; PCE, photothermal conversion efficiency.

* Corresponding author.
E-mail address: alessandro.feis@unifi.it (A. Feis).

https://doi.org/10.1016/j.pacs.2021.100281
Received 21 October 2020; Received in revised form 5 May 2021; Accepted 10 June 2021
Available online 14 June 2021

because light attenuation by living tissues is relatively low at these wavelengths. This fact allows PNPs to be irradiated without excessive interference by cell constituents, thus improving PNP efficiency in those processes of light absorption and energy conversion which form the basis for the use of PNPs in diagnosis and therapy [18,19].

The use of sensitive probes has been particularly beneficial for the advancement of photoacoustic microscopy. In fact, several kinds of photoacoustic microscopy techniques already exist [20], that are being explored for an increasing number of medical applications [21], which vary from two-dimensional imaging to computer-aided tomography [22]. As photoacoustic signal generation occurs upon absorption of the excitation radiation, high absorption coefficients at the excitation wavelength are a favourable feature for PNPs when they are used as contrast agents in living organisms [23–26].

Similar considerations may be made regarding the applications of PNPs in photothermal therapy (PTT). This is a promising kind of treatment for a variety of illnesses, including cancer. A prominent feature is the selectivity of its action, which can damage cancerous cells while leaving normal cells unaffected. The basis for this property is laser irradiation, which can be restricted to a specific body region leading to a localized temperature increase. Extreme localization of the effect can be obtained by conjugating the PTT agent to antibodies that specifically target cancer cells, thus increasing the efficiency and selectivity of the light / PNP interaction at the irradiation wavelength. Photoacoustics is not directly involved in PTT. Nevertheless, the efficiency of the photophysical processes involved in heat generation can be conveniently evaluated – often in a quantitative way – by the use of photoacoustics as a spectroscopic tool. Finally, PAI and light-based therapeutic methods (PTT, photodynamic therapy, and more) can be combined in a fruitful manner [22,27], especially when suitable contrast agents are employed [28–30].

This review covers various aspects of research on nanoparticles. The central question common to the studies presented here can be expressed in the following terms: which properties make PNPs suitable as photoacoustic agents? This is initially discussed in Section 2, which gives an overview of the optical properties of plasmonic systems and their relationship with size and shape. The section is focussed on gold nanoparticles as representative objects. Section 3 is a general presentation of the thermoelastic events triggered by light absorption in dispersed PNPs. These events give rise to the material response generating photoacoustic signals. Two specific parts – Sections 4 and 5 – deal with structural modifications of PNPs and their consequent effect on the photoacoustic response. Section 4 briefly presents examples of surface modifications and their significance in photoacoustic studies. Section 5 discusses the effects of aggregation on the optical spectra of PNPs. Photoacoustic literature is extensively reviewed in Section 6. In particular, by illustration of several examples, it addresses the determination of a property essential for photoacoustic applications, namely, the efficiency of the transduction of light absorption into heat. Methodological aspects constitute the principal focus of the section, hence, for clarity only studies on gold PNPs are presented. The relevance of photoacoustic methods for this purpose is also introduced. The last part of the review – Section 7 – gives a parallel treatment of non-metallic PNPs. It presents photothermal properties of materials based on copper sulfide, and outlines the role of unconventional plasmonic systems as an emerging topic. In fact, the discovery of new materials will enable the design of instruments that can provide new opportunities for photoacoustic and photothermal studies.

2. Optical properties of plasmonic nanoparticles

Some classes of inorganic nanomaterials are characterized by special optical transitions indicated as plasmonic excitations [31]. The term plasmon defines a quasiparticle, or excitation mode, involving the free electrons of the material. Strictly speaking, the excitations involved in plasmonic studies are most often plasmon polaritons. However, the polariton aspect is often implicitly assumed and the simpler term plasmon is commonly used [13].

Size and shape of nanoparticles are directly correlated with the properties of localized surface plasmon polaritons. A characteristic property is the resonance wavelength maximum of the LSPR, which can lie in the ultraviolet, visible, or NIR wavelength range [4,32]. The relationship between the LSPR band position and PNP size became soon apparent in early studies, starting from the cases of Au [33] and Ag [34] nanospheres. The LSPR maximum of these systems shifts to longer wavelengths as the PNP diameter increases. This experimental relationship is in close agreement with the predictions based on a very early general optical theory, i.e., the Mie theory of scattering from nanoparticles [11]. We recall that this theory applies to PNPs that are smaller than the wavelength of the incident light by a factor about 0.1. A simple example of this relationship for Au nanospheres and nanoshells – i.e., “sphere within a sphere” nanostructures – is shown in Fig. 1. On the basis of progress in nanoparticle synthesis, which is not reviewed herein, it soon became evident that anisotropic particles can be especially advantageous. In contrast to spherical objects, they display an even larger tunability of the LSPR maximum [16]. Nanorods, in particular, have been actively investigated for this reason [35–37]. Their shape is primarily described in terms of the aspect ratio, i.e., the ratio between length and width. The left part of Fig. 2 shows how an aspect ratio change of just a few units leads to a ~ 300 nm wavelength shift for the LSPR of the longitudinal mode of gold nanorods [38]. This can be advantageously exploited to produce nanorods with strong NIR absorption, both in the first and the second transparency windows. Recently, still higher aspect ratios have been attained [39,40]. An example is shown in the right part of Fig. 2, where the aspect ratio of “thin” Au nanorods is extended up to 10 and the LSPR maximum shifted beyond 1200 nm, revealing the strong dependence of the LSPR maximum on aspect ratio. The application of this kind of PNP has recently been demonstrated in the generation of photoacoustic signals by laser excitation at 1064 nm [41].

Recent anisotropic structures display branched shapes, e.g., nanotripods [42] and nanostars [43]. In these cases, several geometrical factors determine the LSPR position, among which the number and aspect ratio of the branches and the core size are particularly important. Fig. 3 displays a representative example of the strong dependence of LSPR wavelength upon nanostar size [44]. This relationship between structural and optical properties shows that the LSPR of nanostars can be as easily tuned as that of nanorods, even in the NIR range.

The effect of the three-dimensional nanostructure on the optical properties of PNPs does not only involve the resonance wavelength, but it also determines the resonance strength, which is often expressed as an extinction cross section at the wavelength λ, Q_E (λ). According to a general rule, Q_E increases for larger PNP volumes. In the case of very small PNP dimensions, atomic aggregates are often termed clusters rather than nanoparticles. These systems do not give rise to plasmonic excitations; therefore, they cannot generate photoacoustic signals. At the other extreme (i.e., for sizes larger than the light wavelength) surface plasmon resonances are not localized, unless hybrid nanostructures are formed, e.g. nanospheres on metal films [45]. Therefore, the typical size scale of useful PNPs is of the order of tens of nanometres. The ratio between Q_E and volume has been proposed as a useful indicator of PNP efficiency in heat production, as it takes into account both material properties [46].

Moreover, the chemical composition of the system determines Q_E to a large extent. This results from the dielectric properties of the PNP bulk material, which may be a metal [47,48] or a semiconductor [49]. A smaller contribution arises from the dispersing medium. A third factor that can play a role is the molecular layer that coats the surface of PNPs. The first two aspects will be introduced in Section 3, whereas the third one is presented in Section 4.

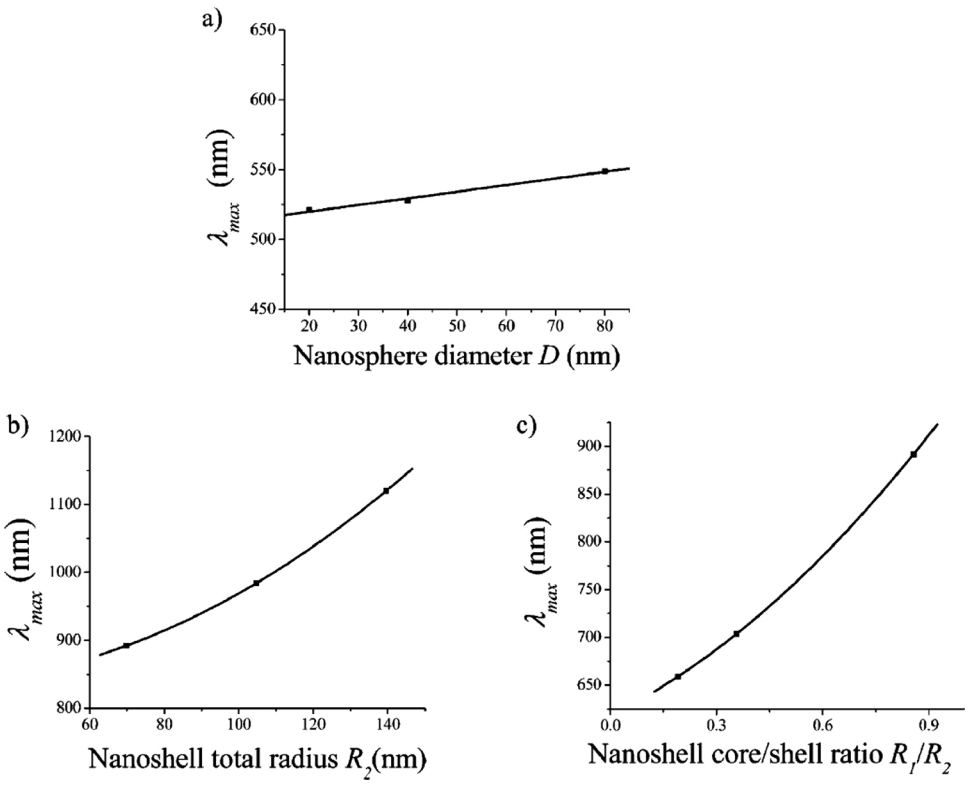

Fig. 1. Calculated position of the LSPR band maximum for representative spherical nanoparticles. (a) LSPR maximum wavelength of gold nanospheres with various diameters. (b) LSPR maximum wavelength of silica (core) / gold (shell) nanoshells with increasing total radius. The ratio of the core radius (R_1) to the total radius (R_2) was kept constant in this calculation at R_1 / R_2 = 0.857. (c) LSPR maximum wavelength of the same kind of nanoshells upon variation of the (R_1 / R_2) ratio. The total radius was constant (70 nm) in this calculation. Adapted from Ref. [4] with permission. Copyright 2006 American Chemical Society.

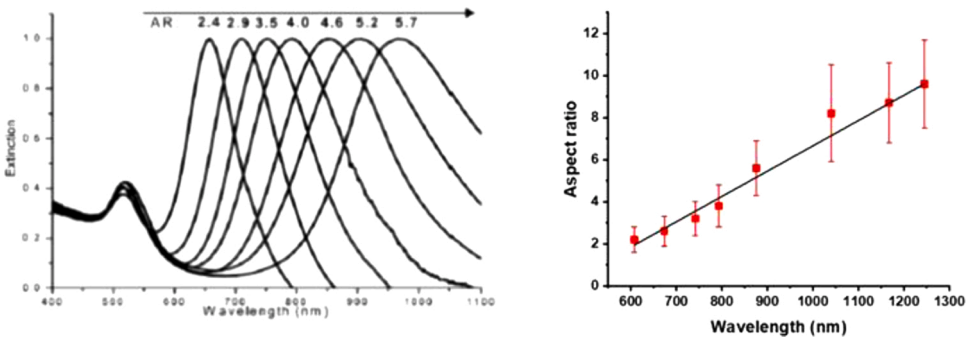

Fig. 2. (*left*) Experimental LSPR extinction spectra of nanorods with an aspect ratio (indicated as AR) increasing from 2.4 to 5.7. Adapted with permission from Ref. [38]. Copyright 2009 Wiley-VCH. (*right*) The dependence of the experimental LSPR maximum on the aspect ratio of specifically prepared "thin" Au nanorods. Length varied from 19 to 93 nm for a width < 10 nm. Adapted with permission from Ref. [39]. Copyright 2018 American Chemical Society.

3. Photoacoustic response of nanomaterials

In the previous section we have briefly reviewed the optical properties of various PNP types, and in particular, we have given a few examples of the extinction spectra of nanostructured Au nanoparticles of various shape and size. Extinction spectra form the basis for the optoacoustic response of both traditional and innovative PNPs [50]. On the other hand, the events generating photoacoustic signals in condensed-phase systems must be considered in a wider picture. This includes the thermoelastic properties of all the phases present in the sample. Most frequently PNPs are investigated as a biphasic system, i.e., solid PNPs dispersed in an aqueous solution as liquid phase. We will consider analogies and differences when the properties of molecular solutions -which are monophasic - are contrasted with those of PNP dispersions.

According to well-known relationships, the photoacoustic signal is primarily determined by the occurrence of light absorption. As it concerns the optical properties of the sample, this can be measured by an absorption cross section Q_A or, equivalently, by an absorption factor α [51]

$$\alpha = 1 - 10^{-A} \quad (1)$$

which is related to the decadic absorbance A. Therefore, enhancing light absorption by increasing Q_A is an important criterion in designing new materials and – in particular – innovative PNPs that can be useful for photoacoustic applications [52]. The extent of light absorption is determined by the number of incident photons, which can be high especially when the signal is generated by laser light [53]. The generation of the optoacoustic signals is also determined by the thermoelastic properties of the sample. In the case of dispersed PNPs, these properties are mainly related to the environment, i.e., the dispersing liquid phase, surrounding the primary absorber. In this context, the relationship between optoacoustic signal and thermoelastic properties of the solvent – or dispersing agent – is identical for molecular solutions and PNP dispersions: it is simply determined by the liquid phase, which is preponderant for dispersions and the only phase for solutions.

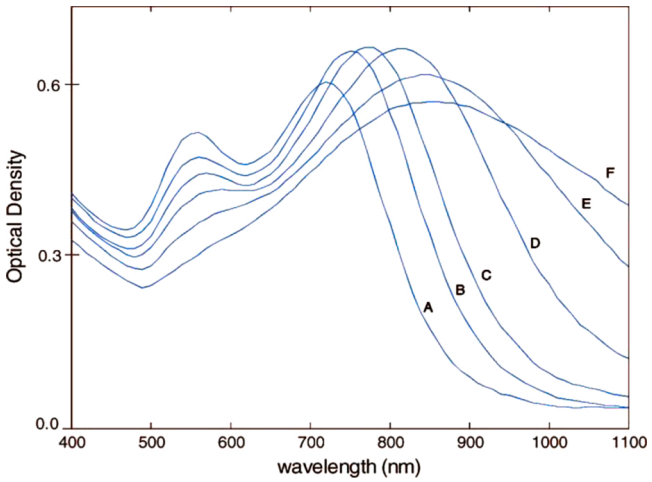

Fig. 3. Experimental extinction spectra of Au nanostars with increasing size. A-F: the number of branches increases from 7 to 14; the core diameter from 27 to 57 nm; the total diameter from 45 to 116 nm. Adapted with permission from Ref. [44]. Copyright 2008 American Chemical Society.

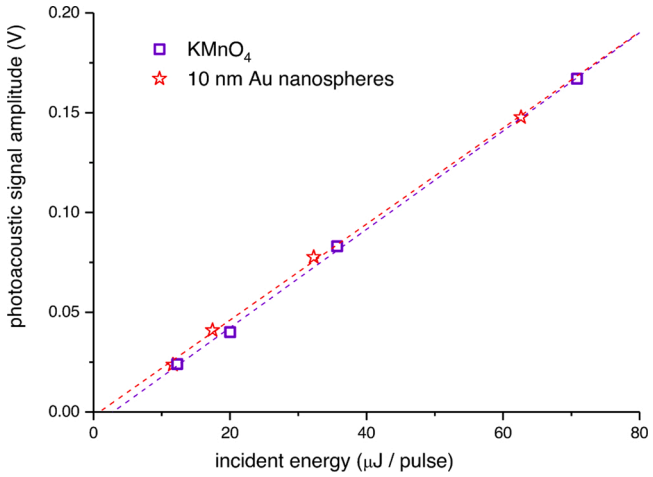

Fig. 4. Photoacoustic signal amplitude as a function of incident laser energy from an aqueous dispersion of 10 nm Au PNPs (stars, 3×10^{-8} M concentration) and a potassium permanganate reference solution (squares, 1.8×10^{-5} M concentration). The excitation wavelength was 532 nm and the laser cross section was 0.1 cm^2. Linear fit of the data (dashed lines) yielded the slope values 2.41 ($\pm$ 0.06) $\times 10^{-3}$ and 2.46 ($\pm$ 0.05) $\times 10^{-3}$ for sample and reference respectively. The figure is adapted from Ref. [59] with permission.

Moreover, the material response is sensitive to the time course of the light excitation pulse [54,55]. In many experimental configurations, the laser-induced pressure change P_0 in an illuminated cylinder will be given by an approximate equation that is valid on the assumption the laser is not focussed [56]:

$$P_0 = \rho \nu^2 \beta \Delta T = \frac{\rho \nu^2 \beta E \alpha}{\pi R_f^2 \rho C_p} \quad (2)$$

where R_f is the radius of the laser beam, E is the laser pulse energy, T is the cylinder temperature and α is as defined above. The following thermoelastic properties of the sample are included: the mass density ρ ; the speed of sound in the medium ν; the volumetric expansion coefficient β, and the heat capacity at constant pressure C_p. This simplified equation displays two significant features of the photoacoustic signal:

i) the signal is related to a light-induced temperature change. This underlines the connection between photothermal properties and optoacoustic measurements, and

ii) the signal originates from light absorption. The consequence is that other optical events – and in particular, resonant and non-resonant scattering by PNPs – do not appreciably influence the signal in a direct way. This has been experimentally verified in turbid dispersions at relatively low concentrations in the case of non-resonant scattering by silica particles [57].

When two phases are present in the material generating the photoacoustic signal, care must be taken to assess subtle effects on the photoacoustic signals. For instance, the measurement of signals from silica-coated Au nanospheres has demonstrated that signal amplitudes are overwhelmingly related to the properties of the dispersing phase [58]. This behaviour is the same as that expected for the signals of molecular solutions. Fig. 4 shows a comparison between the photoacoustic signals of an aqueous solution of potassium permanganate and those of water-dispersed Au nanospheres of 10 nm diameter [59]. Both systems produce signals of the same amplitude within experimental error. We stress that the measurements have been performed under frequently employed experimental conditions, in particular: 10^{-8} s laser excitation, low incident light energy and very diluted samples. Different results would possibly be observed for optoacoustic determinations employing shorter laser pulses and higher photon energy.

Deviations from the expected signal behaviour derive mainly from i) the time scale of the processes involved in signal generation and ii) non-linear response in relation to laser fluence [60,61]. The time course of photoexcitation and acoustic signal generation is schematically presented in Fig. 5.

A similar description has been reported previously [54] for the photothermal excitation of dispersed metal PNPs. The fastest process is electron gas thermalization, which occurs within 10^{-13} s. This is followed by electron-phonon interactions, leading to a relaxation process with a time constant of a few ps. Heat diffusion starts with subsequent heating of the medium varying from 10^{-10} s up to 10^{-8} s. The ability to assess whether the three steps are sequential is determined by the duration of the laser pulse. In fact, it can be expected that the three processes overlap for nanosecond pulse excitation, which is a typical condition in photoacoustic measurements.

The time-resolved heat response of PNPs can be computationally simulated. For example, the response of Au nanoshells has been determined according to models which are related to the above description for light excitation with different pulse duration [62,63]. Besides theoretical descriptions of the photoinduced thermal processes, numerical simulations have been employed to study PNPs as photoacoustic signal generators [64]. The above-described approaches are valid until non-linearities arise in the laser / PNP interaction, thereby influencing the photoacoustic signal [61]. This possibility has been described both theoretically [65,66] and experimentally [58,60,67–69]. Several adjustable experimental conditions determine signal non-linearities, including the laser pulse characteristics and PNP concentration. Recent experimental results show that silica coating prevents the occurrence of fluence-dependent non-linearity for the signals generated by relatively large (116 nm diameter) Au nanospheres [70].

In the class of anisotropic PNPs, we first consider Au nanorods as a prototypical case. Versatility of their optical properties is accompanied by a higher complexity if these structures are compared to spherical PNPs. In fact, the geometric anisotropy of the PNP creates an anisotropic heat generation. Fig. 6 shows the computed spatial distribution of the heat power generated by a Au nanorod at different excitation light wavelengths [54]. This example demonstrates that photoacoustic signal generation in anisotropic PNPs is a multifaceted process. In fact, the available experimental results, which will be discussed in Section 6, show high variability of the efficiency of heat generation for nanorods and other anisotropic systems. More materials displaying different degrees of anisotropy have been increasingly proposed and tested in recent years. In particular, hollow PNPs offer manifold geometrical parameters potentially leading to a superior control of the LSPR wavelength

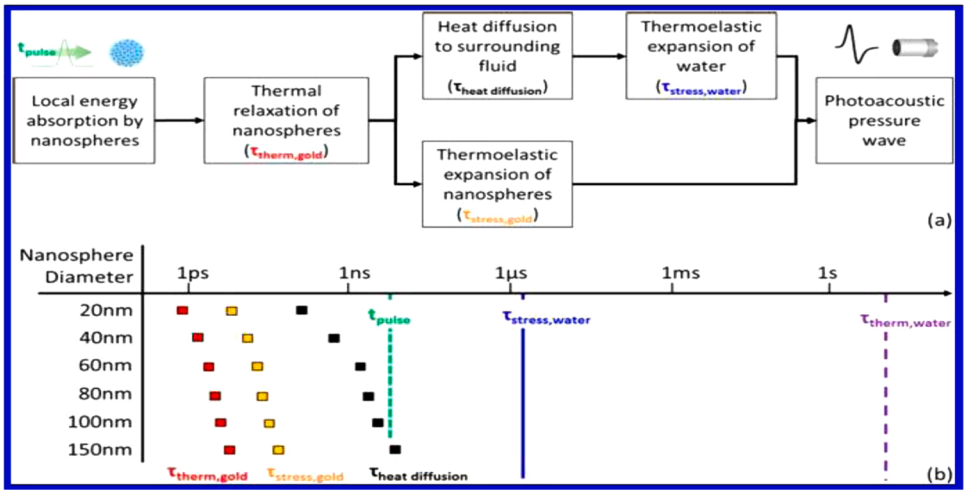

Fig. 5. (a) Schematic representation of the events leading from light absorption to photoacoustic signal generation in a PNP aqueous dispersion. (b) Time course and microscopic interpretation of the above events. $\tau_{\text{therm, gold}}$ and $\tau_{\text{stress, gold}}$ are fast time constants on the photoacoustic signal time scale when the excitation pulse is of the order of ns. The same is true of $\tau_{\text{heat diffusion}}$ for most nanoparticles. Thermoelastic expansion of water is the main determinant for signal generation. Adapted with permission from Ref. [60]. Copyright 2016 American Chemical Society.

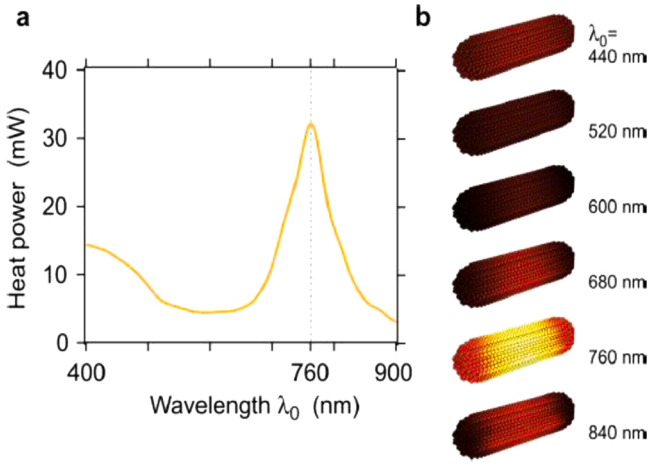

Fig. 6. (a) Calculated wavelength-dependent heat power of a Au (50 × 12 nm) nanorod. (b) Spatial distribution of the heat power density at different wavelengths. Adapted from Ref. [54] with permission. Copyright 2012 John Wiley and Sons.

maximum and intensity distribution. For example, nanocages are an innovative material that can be obtained from cubic PNPs by targeted synthetic methods [71]. Their application in PAI has been successfully performed [72] and, when properly functionalized, they allowed an *in vivo* sensitivity below 0.5 nM to reached for 778 nm excitation [73][1] . Assembled PNPs can equally lead to a specific degree of anisotropy. Stacked disks have been proposed as advantageous contrast agents because they can be used for both PAI and applications based on light scattering, depending on the wavelength [74].

4. Surface chemistry of nanoparticles

The properties of the objects under review herein are not just defined by the size and overall shape of PNPs: they are rather related to structural features, e.g. spikes, or cavities, at the nanometer scale (typically from 10^{-8} to 10^{-7} m). The whole particle, of course, may also be in this size range. An important consequence of nanostructure is that an exceptionally high number of atoms are exposed at the particle surface. The importance of this quality was recognized early in studies on the physics of plasmonic excitations [11]. In addition, it is the surface of PNPs which primarily interacts with biological systems [75,76]. The role of surface properties in the biological activity of PNPs has been a key factor in the recent explosive development of nanoparticle science [50].

Surface properties of nanoparticles can be engineered in several ways. A classical case consists in tuning the LSPR wavelength by varying the refraction index at the PNP surface [77]. For instance, this effect is fundamental for analytical methods like surface plasmon resonance. On the other hand, shifts in the LSPR maximum, which may be obtained by variations of PNP shape and aggregation, are larger by orders of magnitude. Therefore, refraction-index induced changes can be considered as secondary effects in PNP resonance tuning from a photoacoustic standpoint.

Other kinds of surface modifications can yield an even stronger impact. The inorganic surface of PNPs can be functionalized through beneficial, often irreversible chemical reactions [78]. In fact, the PNP surface cannot be viewed as a "bare" metal or semiconductor interface in most cases [29]. When nanoparticles are obtained by chemical synthesis, excess reagents and / or capping agents stay adsorbed at the interface between nanoparticle and solvent for very long times. In some cases, these chemicals may be replaced or further reacted [79]. Surface chemical modification can lead to improved solubility in water, and various kinds of organic solvents, or to a better stability in biological fluids. However, toxicological issues related to the coating must be avoided [80]. Moreover, changing the coating of semiconductor nanoparticles is a versatile tool to move the LSPR maximum, or even drastically change its strength by altering the electronic structure of the main constituent [81,82].

Linking a protein [20] or an aptamer [83] to the PNP surface may change its affinity towards a target molecule, or a whole cell, allowing an improved PAI sensitivity and selectivity [8]. The experimental results reported in Fig. 7 show how cancer cells can be multi-targeted, meaning they can be differently imaged by PAI upon changing the excitation wavelength. This is attained by coupling two different kinds of photoacoustic contrast PNPs (namely, Au nanorods with extinction maximum close to either 785 nm or 1000 nm) to antibodies with a specific affinity towards two different proteins: either HER2, human epidermal growth factor receptor 2, or EGFR, epidermal growth factor receptor. Both proteins are involved in the development of tumours. A good photoacoustic contrast was obtained for *in vivo* concentrations of 1.5 nM [84].

Finally, the effects of silica coating on metal PNPs are being currently explored also in view of biomedical applications [85]. This kind of coating displays advantageous stability and reduced chemical reactivity at the PNP surface. Importantly, the reduction of the photoacoustic signal by the coating is within tolerable limits under the laser excitation

[1] When *in vivo* molarity or mass content are quoted in this review, concentrations are estimated on the basis of a mouse blood volume V = 2 mL.

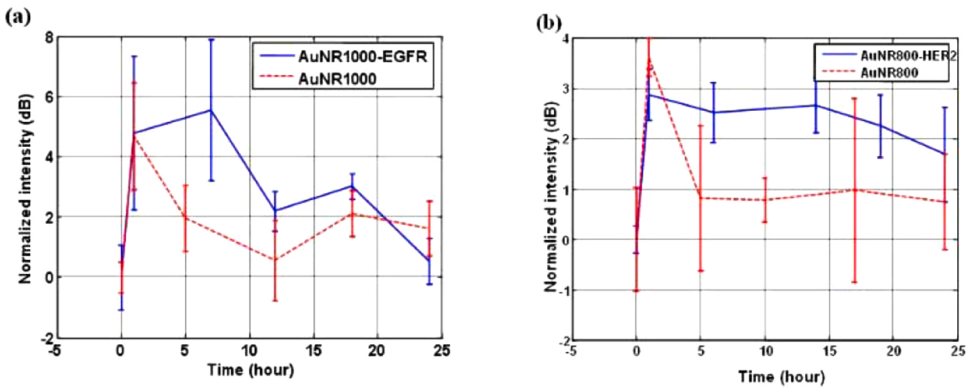

Fig. 7. PAI intensity as a function of time after *in vivo* injection of Au nanorod-based contrast agents. Two types of PNPs with LSPR at 1000 nm or 785 nm were specifically functionalized to bind the receptors EGFR or HER2, respectively (see the text for the meaning of the abbreviations). (a) Continuous line: signals from EFGR-functionalized Au nanorods. Dashed line: reference signals from non-functionalized Au nanorods. Laser excitation wavelength 1064 nm. (b) Continuous line: signals from HER2-functionalized Au nanorods. Dashed line: reference signals from non-functionalized Au nanorods. Laser excitation wavelength 800 nm. Reprinted with permission from Ref. [84]. Copyright 2008 Optical Society of America.

conditions that are usually employed for PAI and photoacoustic spectroscopy.

5. Aggregation effects on the optical and photoacoustic properties of nanoparticles

A fundamental property of PNPs, i.e., the extinction cross section Q_E (λ), has been introduced in Section 2. In view of the presentation of photothermal properties in this and the following sections, it is useful to consider separately the two contributions which add – often to a different extent – to give Q_E, i.e., the absorption cross section, Q_A, and the scattering cross section, Q_S:

$$Q_E(\lambda) = Q_A(\lambda) + Q_S(\lambda) \quad (3)$$

Q_A is the only term that contributes to the photothermal processes which are being reviewed. Hence, knowing the extent of absorption within extinction is an important piece of information in the characterization of photoacoustic properties [59]. Remarkably, the wavelength dependence of Q_A and Q_S is not governed by the PNP size only. It also depends on the aggregation of PNPs into closely spaced dimers, trimers, and higher aggregates [86], as has been demonstrated by simulations and experimental results [87].

We first review the properties of the simplest PNP aggregate, namely, the nanosphere dimer. It was soon recognized that the optical (and optothermal) properties of a nanosphere dimer are related to a spatial parameter: the interparticle gap, i.e., the distance between the surfaces of each constituent monomer [13,88,89].

Fig. 8 is particularly explicit as it shows the strong dependence of Q_A on the nanoparticle separation. The role of the interparticle gap essentially derives from plasmonic excitation coupling [90]. By exploiting this effect, an interesting analogy has been proposed between the case of molecules and their constituent atoms, and that of aggregated PNPs and PNP monomers [91]. Interparticle plasmon coupling has an effect not only on the extinction strength but also on the LSPR position: this makes the engineering of PNP aggregates almost as powerful in determining the optical properties as the design of the shape and size of plasmonic PNPs that has been outlined in the previous sections. An additional important influence on the optical properties also stems from the geometrical features of the monomers composing the PNP aggregates. This is clearly displayed by calculated and experimental scattering spectra of variously shaped Au dimers, e.g., ideally spherical vs. irregularly shaped PNPs [92,93].

Higher-order aggregates have also been investigated. Linear aggregates of 2–6 Au nanospheroids have been prepared by electron beam lithography [94]. Self-assembled chains of identical Au PNPs – with an average diameter of 14 nm – have been obtained and stabilized in aqueous dispersion by polypyrrole coating of preformed nanospheres [95]. In addition, unusual PNP aggregates can be obtained by combining various geometrical and optical features. Fig. 9 shows an example of the spectral properties of an unusual trimer, for which the calculated spatial distribution of heat generation was also reported [96].

Turning now to the photoacoustic properties of PNP aggregates, it can be expected that they are dominated by interparticle interactions when the gaps between the constituent PNP monomers are sufficiently small. Experimental studies based on photoacoustic methods are still lacking for plasmonic model systems. On the other hand, recent reports by photothermal absorption spectroscopy have revealed – at the single nanostructure level – significantly divergent spectral distributions of Q_A

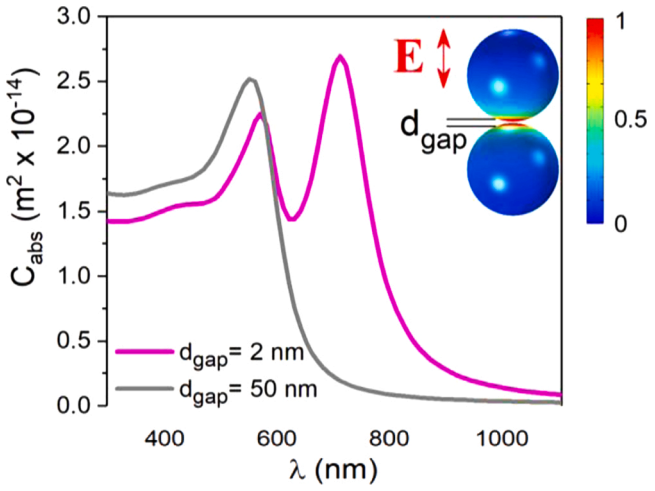

Fig. 8. Wavelength-dependent Q_A for Au (d = 40 nm) nanosphere dimers separated by 2 and 50 nm. The inset shows the spatial distribution of the electric field amplitude for the indicated polarization. Adapted with permission from Ref. [89]. Copyright 2019 American Chemical Society.

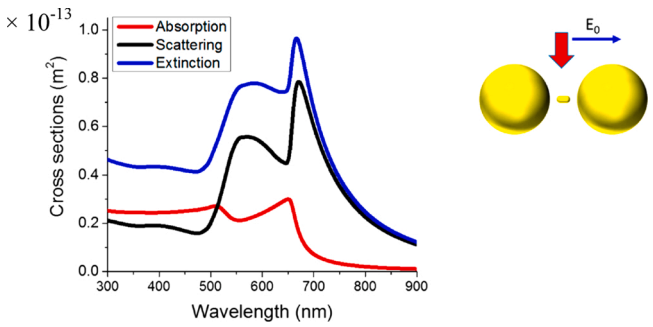

Fig. 9. Wavelength dependence of the cross sections Q_A, Q_S and Q_E for a trimer formed by two Au nanospheres (d = 100 nm) and one Au nanorod (10 × 20 nm) separated by a 40 nm gap. The polarization of the incident electric field is indicated. Adapted with permission from Ref. [96]. Copyright 2016 American Chemical Society.

and Q_S in a PNP decameric aggregate [97] and in variously shaped Au nanorods [98]. Moreover, it has been shown that PNP aggregation can favourably change the photoacoustic properties of Au nanospheres when they interact with biological materials. To demonstrate this valuable interaction, Au PNPs have been functionalized with antibodies targeting the surface of cancer cells. This modification leads to selective PNP accumulation at the cell surface resulting in close contacts that determine a red shift of the LSPR band, which can be assigned to interparticle coupling. In addition, this change in the optical properties has been exploited to increase the photoacoustic signal used for *in vivo* imaging [99], yielding good contrast at a concentration of 250 μg / mL. PNP aggregation has been suggested to be the reason for photoacoustic signal enhancement also in the case of simpler surface modification [100,101].

6. Photothermal conversion by metal nanoparticles

PNPs are distinctive in photoacoustics because the energy relaxation channels following light absorption are different from the pathways displayed by molecules, both in extent and time scale [102,103]. In fact, molecules display a manifold of non-radiative pathways, e.g., inter-system crossing, internal conversion, and photoinduced reactions. Conversely, these events do not occur in PNPs, or are seldom relevant. The same can be said of radiative pathways, which normally lead to a very low emission quantum yield in PNPs. In conclusion, once a photon is absorbed by a PNP, the conversion of the photon energy into heat should occur with a yield close to unity. The efficiency of this process is currently an important field of both fundamental and applied research. In fact, the quest for new photoactive materials characterized by high conversion efficiency constitutes a major goal in cancer therapy through photothermally induced biological effects [104–107]. Additionally, several kinds of PNP are "dual", in that they can be used for both photothermal therapy and photoacoustic imaging [108–110]. Au PNPs have also led to improvements in an extremely sophisticated kind of PAI, belonging to nanothermometry methods [111].

When new plasmonic systems are developed, a significant hindrance is often encountered. If the LSPR intensity reaches a maximum at long (e.g. NIR) wavelengths, photothermal conversion can be surprisingly low – especially for gold-based materials [112]. Nevertheless, many recently developed metal PNPs display both extremely broad tunability – up to a wavelength of 1700 nm [17] – and very high photothermal conversion: both advantages depend on the shape of the PNPs, among other factors. Nanostars are a noteworthy example of this versatility, which results from the combined optothermal effects deriving from core dimensions, and size / number of spikes [113,114]. Similarly, nanorods [115] and nanoshells [89] display strong size effects which allow their LSPR to be tuned over a wide range. To illustrate the potential of such differently shaped PNPs, some representative cases are reported and discussed below. It is not possible to review the photothermal properties of all PNP types, therefore, we have chosen to focus on representative examples of gold-based PNPs in this section.

It should be noted that the determination of photoconversion can be made under different experimental configurations, to evaluate either macroscopic – i.e., ensemble – properties, like temperature changes, or microscopic properties like molecular or PNP cross sections. Accordingly, we group different kinds of measurements as microscopic when they are not based on thermometry. Importantly, a significant fraction of this class of methods includes photoacoustic methods.

Macroscopic determinations often consist in a very accurate temperature measurement of light-irradiated PNP samples. For instance, a PNP dispersion is placed in a quartz cell and the temperature is recorded by a thermocouple clamped to the cell. Temperature variations are periodically recorded during laser illumination and dark relaxation intervals. The output of these studies is often defined as photothermal conversion efficiency (PCE). Data analysis must include instrumental parameters, as shown in the following equation [116]:

$$\eta = \frac{hA(T_{max} - T_{amb}) - Q_0}{I\left(1 - 10^{-A_\lambda}\right)} \quad (4)$$

where η is identified with PCE in this study and in correlated investigations, which will be presented below. h stands for a heat transfer coefficient and A is the cell surface. T_{max} and T_{amb} are the maximum temperature reached by the system and the ambient temperature, respectively. Q_0 is a correction term due to light absorption by the quartz cell and the solvent. I represents the incident laser power. A_λ is the sample absorbance given by the Beer-Lambert's law, $A_\lambda = \varepsilon_\lambda L$ c, where ε_λ is the molar extinction coefficient, L the optical pathlength and c the molar concentration. It should be noted that the quantity A_λ is actually the extinction measured at the spectrophotometer, as also remarked in [117].

An alternative opportunity is offered by direct thermocouple immersion in the dispersion. The latter configuration minimizes heat losses through the cuvette and sample holder [118]. Notably, this difference in the experimental design has led to an order-of-magnitude change in the accuracy of PCE determination. Owing to its relevance in wide ranging applications, macroscopic analyses have been applied both *in vitro* and *in vivo* to estimate the potential of new PNP-based materials [89,119].

Studies at the microscopic level are currently being developed and involve experiments on single PNPs [120], arrays of PNPs [121], or PNP dispersions [122]. In contrast to macroscopic PCE measurements, the efficiency of the photoconversion at the microscopic level is the ratio between cross sections, Q_A (λ) / Q_E (λ). It must be stressed that the experimental determination of these quantities does not necessarily require measurements on single PNPs. If ensemble observables are properly analysed, they can be related to individual PNP properties. Similar considerations are commonly applied, for example, to determine fluorescence quantum yield or oscillator strength.

The experimental measurements are often substantiated by the calculation of optothermal properties according to various models [123]. We note that both macroscopic and microscopic experimental measurements are often limited by the availability of only a single excitation wavelength. In contrast, calculations allow the expected wavelength dependence of Q_A (λ) / Q_E (λ) to be predicted.

Table 1 displays a demonstrative example of different experimental and calculated photoconversion values. The data collection originates from a study of Jiang et al. [124], where both accurate macroscopic and microscopic approaches are systematically contrasted, allowing an evaluation of the size dependence of PCE in Au nanospheres. Notably, the agreement between the macroscopic and calculated data sets can only be considered to be qualitative, notwithstanding the high accuracy of their determination. It appears that experimentally determined PCE is systematically lower than the calculated Q_A / Q_E ratio. Future studies on the physical origin of this difference may be useful for a better understanding of the subjects treated in both this and the following sections. We remark that this issue has been presented in a previous review [119] on the basis of the comparison among different experimental and computational approaches.

Photoacoustic studies in the field of photothermal properties do not

Table 1
Experimental PCE and calculated Q_A / Q_E ratio of Au nanospheres with increasing diameter. Experimental data from Ref. [124].

Au nanosphere experimental diameter from scanning electron microscopy	Experimental PCE macroscopic determination (η) according to Eq. (4)	Mie-theory calculated Q_A / Q_E at 532 nm (diameter of the model nanosphere)
4.98 ± 0.59	0.803 ± 0.008	0.999 (5 nm)
15.38 ± 1.29	0.784 ± 0.008	0.996 (15 nm)
18.77 ± 0.77	0.737 ± 0.021	0.992 (19 nm)
40.29 ± 2.28	0.694 ± 0.005	0.928 (40 nm)
50.09 ± 2.34	0.650 ± 0.012	0.869 (50 nm)

involve temperature measurements and rather rely on the evaluation of the amplitude of a calibrated optoacoustic signal, as shown in Fig. 4. Therefore, they can be viewed as intrinsically microscopic experimental determinations. In this approach, a suitable standard is employed for the calibration, i.e., a molecular solution with known thermodynamic properties. The latter substance is often termed a calorimetric reference. The experimental photoacoustic conditions for sample and calorimetric reference must be identical. This essentially means that: i) the extinction of sample and reference has to be equivalent, ii) the efficiency of the photoacoustic setup does not vary during the measurements, and iii) both sample and reference are excited by light in the linear regime [53].

Table 2 reports a selection of photothermal properties obtained from aqueous dispersions of Au PNPs by various experimental and computational methods. An overview of the observed variations in different systems is pertinent to our aim, as photothermal conversion is pivotal for the generation of photoacoustic signals. As a first instance, PCE data are presented for several representative kinds of Au nanorods. In most cases, the data were obtained by macroscopic determinations, namely, by an analysis of the temperature increase of dispersions upon laser irradiation. The PCE of two nanorod forms [125,126], obtained in different laboratories at 800 nm and 980 nm, appeared markedly similar. Both values were relatively low, namely, below 0.24. It must be stressed that a strong divergence between calculated Q_A / Q_E values (0.93) and experimental PCE determinations ($\eta = 0.55$) had also been previously described in the case of Au nanorods [36]. In contrast, a microscopic determination employing photoacoustics showed a good overlap between experimental and calculated values of small-nanorod dispersions [127]. Fair agreement between calculated and experimental data was also observed when nanothermometry by quantum dot fluorescence was applied to Au nanorods [128]. Importantly, nanothermometry has been extended to various kinds of Au PNPs, unveiling the effects of shape and size on microscopically determined efficiencies [103,129]. The importance of polydispersity on PCE has been recently reported for Au nanorods and contrasted with the case of Au nanospheres [130].

In many cases the photoconversion process is weakened by energy losses due to light scattering. This is a general aspect of the interaction between light and PNPs, and it becomes increasingly relevant as the PNP size becomes a considerable fraction of the light wavelength [13]. This apparent loss can be compensated in the case of sizeable PNPs displaying complicated forms. In a representative study, the photothermal properties of a new class of branched gold PNPs, i.e., nanohexapods, was studied [114]. The photoacoustic signal of nanohexapod dispersions was calibrated by using that of the dye molecule indocyanine green, a well-known photothermal standard, at 805 nm excitation. The experimental Q_A / Q_E ratio was 0.91, in good agreement with the value computed by the discrete dipole approximation method (0.96). Macroscopic efficiencies were also measured and contrasted for gold nanohexapods, nanorods and nanoshells of comparable size in the same study.

Au / SiO_2 nanoshells represent a PNP class that displays both a fairly high Q_A / Q_E ratio and NIR tunability. Photoacoustic methods were employed to assess these important properties at the microscopic level. Relatively small-sized nanoshells displayed an especially high heat release when excited on the blue side of the LSPR extinction band [131]. Successively, three kinds of nanoshells with different overall size and Au shell thickness were investigated [132]. The Q_A / Q_E ratio was evaluated over an extensive wavelength range (440 − 900 nm). This unusually broad spectral range allowed the contributions of scattering and absorption to extinction (see Eq. 3) to be separated, showing that the smallest nanoshells were most effective, yielding a value of 0.77 at ∼ 600 nm.

Au nanomatrioshkas can be viewed as an extension of the above described nanoshells, as they can involve, e.g., successive Au / SiO_2 / Au nanostructured layers [133]. They combine the advantages of small size and NIR tunability with the additional degree of freedom offered by the third layer. Moreover, the scattering to extinction ratio can be varied over an appreciably wide range [134]. All these features can be exploited in the optimization of nanomatrioshkas as PNPs for optical and optothermal applications.

Besides spherical and cylindrical structures, PNPs with branched shapes have been actively investigated in order to obtain systems displaying both high PCE and broad tunability. In this context, nanostars are especially attractive. Recent work has reported a very high conversion efficiency at ∼ 1000 nm, which was obtained for specifically designed Au nanostars. The latter were formed by a medium-sized core and rod-shaped branches. Besides the size characteristics, the number of branches per PNP proved to be determinant for photothermal properties [113]. It can be envisaged that this kind of metal PNPs – as well as those displaying unusually complicated forms [117,135] – will become a valuable material for photothermal applications. On the other hand, it should be noted that transposing reported values – determined *in vitro* – to *in vivo* efficiency is not obvious. This issue has been seldom treated. Recent work systematically compared photothermal heating before and after cell internalization [136]. Four types of Au PNPs were examined and significant differences were observed for the same PNPs in water and within cells. These changes were explained on the basis of endosomal confinement.

To complete this section, we mention the role of all-optical techniques employing light scattering to evaluate Q_S / Q_E ratio. These methods can be viewed as complementary to photoacoustic determinations. Measuring the contribution of scattering to extinction, in fact, is expected to be consistent with the absorption fraction of the extinction [137,138].

7. Photothermal conversion by innovative plasmonic nanomaterials

The quest for new materials for PNPs which display extended tunability, high photothermal conversion, low costs and reduced toxicity is currently an active area of research [1,139–142]. Attempts have been centred on the substitution of PNP classic materials, i.e., coinage metals, by semiconductor compounds. This choice has been stimulated by the need for LSPR transitions that cover the infrared range to a large extent. Study of the plasmonic properties of various copper sulfide compounds has become a particularly dynamic field [49, 143–145]. Therefore, we will mainly review the optical and photothermal properties of the latter materials, and the photoacoustic studies which employ PNPs based on them.

In order for copper sulfide to display a LSPR band, its Cu:S stoichiometric ratio must follow certain rules. A demonstrative example is shown in Fig.10, where the extinction spectrum of as-synthesized Cu_2S nanorods is featureless in the NIR range. The creation of Cu vacancies gives rise to a progressively more intense LSPR band [146]. This is consistent with the general observation that PNPs with a stable (1:1) CuS stoichiometry display broad LSPR extinction bands in the NIR range. Additional methods to regulate LSPR properties, including temperature-induced processes and surface reactions, have been recently reviewed [147].

Fig. 11 displays an instructive comparison between the calculated optical properties of coinage metals and those of (1:1) copper sulfide [148]. The real part of the CuS permittivity displays a wavelength dependence which changes from positive values (for $\lambda < 673$ nm and $\lambda <$ 1047 nm, depending on the spatial component) to negative values. This suggests that a LSPR is expected only in the NIR range. The absolute values of both the real and imaginary part of the CuS permittivity are considerably smaller than those of metals at infrared wavelengths. The calculated permittivity allows the simulated extinction spectra (which are equivalent to absorption spectra for small nanoparticle size) to be in good agreement with the experimental observations.

The next critical step towards the use of CuS PNPs in photothermal applications is to assure high values of their PCE [149]. It is apparent from inspection of Table 3 that the PCE of this material is extremely

Table 2
Photothermal properties of selected Au PNPs.

Material	Coating agent	Size, LSPR maximum	Q_A / Q_E (method)	Observed ΔT, macroscopic PCE (η) according to Eq. (4)	Excitation wavelength, irradiation conditions	Ref.
Au nanorods	CTAB	50 × 15 nm 845 nm		~ 10 K η = 0.237	980 nm, cw 0.51 W / cm^2 600 s	[125]
Au nanorods (*commercial source*)	PEG	23 × 7 nm ~ 760 nm		22 K η = 0.21	800 nm, cw 2 W / cm^2 1800s	[126]
Au nanorods	Surfactant mixture	44.0 ± 7.9 × 19.8 ± 6.5 nm 638 nm	0.87 ± 0.11 (PA) 0.85 (calculated)		638 nm, pulsed < 15 ns pulses 10 Hz repetition rate	[127]
Au nanorods (*commercial source*)		47 × 24 nm 808 nm	0.98 (quantum dot fluorescence) 0.91 (DDA calculated)		808 nm, cw 5 × 10^3 – 4.31 × 10^5 W / cm^2	[128]
Au nanorods	CTAB	38 ± 3.8 × 10 ± 1 nm ~ 750 nm	0.873 (light scattering) 0.945 (FEM calculated)		750 nm, cw 30 mW / cm^2	[52]
Au nano-hexapods	PVP	25.3 ± 0.9 nm (core) 16.3 ± 2.2 nm × 13.6 ± 1.8 nm (arms) 805 nm	0.91 (PA) 0.96 (DDA calculated)	36.5 K	805 nm, pulsed < 15 ns pulses 10 Hz repetition rate (PA method) 808 nm, cw 0.8 W / cm^2 300 s (macroscopic method)	[114]
Au/silica nanoshells	3-amino-propyl-triethoxy-silane	d = 24 ± 3 nm, d = 29 ± 3 nm, (total diameter, bimodal distribution) ~ 800 nm	0.97 ± 0.05 (PA)		532 nm, pulsed ~ 7 ns pulses,10 Hz repetition rate ~ 7 mJ / cm^2	[131]
Au/silica nanoshells	PVP	d = 76 ± 18 nm (core diameter) d = 118 ± 30 nm (total diameter) ~ 660 nm	0.77 ± 0.13 (PA)		780 nm, pulsed ~ 10 ns pulses, 10 Hz repetition rate < 70 μJ / cm^2	[132]
Au/silica nanoshells		d = 120 ± 5 nm (core diameter) l = 10 ± 1 nm (shell thickness) ~ 870 nm	0.68 ± 0.03 (fluorescence thermometry)		808 nm, cw < 2 × 10^5 W / cm^2	[129]
Au/silica/Au nano-matrioshkas		d = 88 ± 5 nm (total diameter) 783 nm		30 K η = 0.63	810 nm, cw 2 W / cm^2 2400 s	[133]
Au nanostars	PEG	52 ± 5 nm (core diameter) 65 ± 10 nm × 24 ± 5 nm (spikes) 1120 nm		38 K η = 0.788	980 nm, cw 1.8 W / cm^2 360 s	[113]
Au nanostars	CTAB	38 ± 4 nm (core diameter) 46 ± 6 × 9 ± 3 nm (lobes) 820 nm	1.02 ± 0.03 (fluorescence thermometry)		808 nm, cw < 2 × 10^5 W / cm^2	[129]
Au nanostars	PVP	36 ± 4 nm (core) 13 ± 3 × 6 ± 3 nm (lobes) 780 nm	0.43 ± 0.05 (fluorescence thermometry)		808 nm, cw < 2 × 10^5 W / cm^2	[129]
Au nanostars	PVP	25 ± 2 nm (core) 10 nm (arms) ~ 750 nm	0.957 (light scattering) 0.971 (FEM calculated)		750 nm, cw 30 mW / cm^2	[52]
Au rugged hollow spherical PNPs	PEG	d = 90 ± 10 nm (external) ~ 710 nm		11.7 K η = 0.97 ± 0.01	790 nm, cw 1 W / cm^2 1800s	[117]
Au nano-bellflowers	PEG	d = 314.3 ± 27.6 nm (hydrodynamic) > 1000 nm		72.8 K η = 0.74	808 nm, cw 1.1 W / cm^2 3000 s	[135]

Abbreviations used in the table: CTAB, cetyl trimethylammonium bromide; cw, continuous wave; PEG, polyethylenglycol; PA, photoacoustic; DDA, discrete dipole approximation; FEM, finite element method; PVP, polyvinylpyrrolidone; d = sphere diameter.

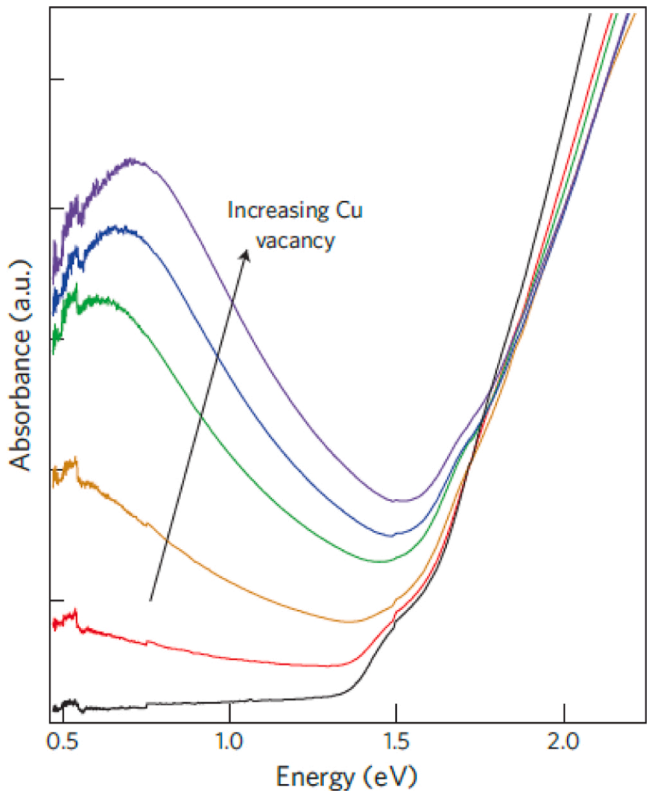

Fig. 10. Experimental LSPR spectra of Cu(I)S nanorods. The spectra indicate that plasmonic excitation is the determinant for the NIR band of this material. The latter band is absent when the stoichiometry is (2:1) Cu:S in the as-synthesized sample. Exposure to oxygen leads to Cu vacancies that facilitate plasmonic excitations [146]. Reprinted by permission from Springer Nature: copyright 2011 Macmillan Publishers Ltd.

variable, with values in the range from $\eta = 0.25$ to $\eta = 0.93$. To our knowledge, experimental PCE values close to unity have not been observed until recently for CuS-based nanomaterials [150]. The structural determinants that cause this variability have not yet been completely rationalized. The very high accuracy of the experimental data reported in the latter study prompted the proposal that experimental conditions, particularly PNP concentration and dispersing phase properties, influence PCE.

One of the earliest CuS-based theranostic systems displayed favourable features for both PTT and positron emission tomography [151]. Subsequently, CuS spheroids were tested as efficient contrast agents for PAI with 1064 nm excitation, i.e., at the fundamental output wavelength of Nd YAG lasers. The wide availability of such lasers favours extensive use of this approach in medical applications [152–154]. Fig. 12 displays a representative application of CuS spheroids for *in vivo* PAI.

Tian et al. were able to shift the LSPR resonance to long wavelengths by synthesizing hexagon-shaped CuS nanoplatelets. In addition, they improved the photothermal properties at 980 nm excitation through assembling these systems into a flower-like shape [155]. The same research group measured the macroscopic PCE of non-stoichiometric Cu_9S_5 platelets, which had been synthesized to yield efficient photothermal agents, obtaining an efficiency of 0.257 at 980 nm [125]. Much higher PCE at the same wavelength (0.567) was observed successively for PNPs with a different stoichiometry, namely $Cu_{7.2}S_4$ [156]. Shape effects were proposed to foster the very high PCE (up to 0.748 at 980 nm) of CuS assembled nanobundles [157].

Copper sulfide PNPs can display LSPR bands at still longer wavelengths. A recent study has reported the experimental macroscopic PCE of CuS nanorods and Cu_9S_8 nanodots. Both PNPs displayed a fairly high efficiency, 0.366 and 0.490 respectively, at 1064 nm excitation [158]. Suitability of CuS nanodisks and nanoprisms as PAI contrast agents was demonstrated at excitation wavelength of 920 nm for ovarian cancer imaging with an *in vivo* concentration of 5.4 nM [159]. Our laboratory exploited a photoacoustic method to attain the determination of the Q_A / Q_E ratio of covellite CuS nanoflakes for 1064 nm excitation. The PNPs had been dispersed in water and after subtraction of the solvent contribution a high ratio (0.76) was determined [160].

A wavelength dependence has been demonstrated for the PCE of small, PEG-capped CuS nanospheroids [161]. The error limits in this determination were below 0.058. The measured PCE values were in the range $0.65 - 0.71$ at 806 nm and 0.58 at 970 nm. The decrease at longer wavelength is related to an experimental effect, which was probed by isotopic H_2O / D_2O replacement. Importantly, light scattering contributions to the wavelength dependence were ruled out on the basis of calculated optical properties.

PTT applications of CuS PNPs are becoming increasingly common. CuS-based contrast agents include composite materials that couple CuS and coinage metals, e.g. Au nanospheres on CuS platelets [162], Au / Cu_7S_4 hetero-structured nanorods [163], Au / Cu_9S_5 hybrid nanospheroids [164]. Their PCE value can be high in the NIR region, as reported in Table 3.

The versatility of CuS-based materials does not imply that they are the only non-metal PNPs which can be useful in photothermal applications. New characteristics can be sought in other kinds of materials. Copper selenide PNPs have already been tested both *in vitro* and *in vivo*. Low (~ 8 nM) concentrations were effective in rat forearm at 900 nm

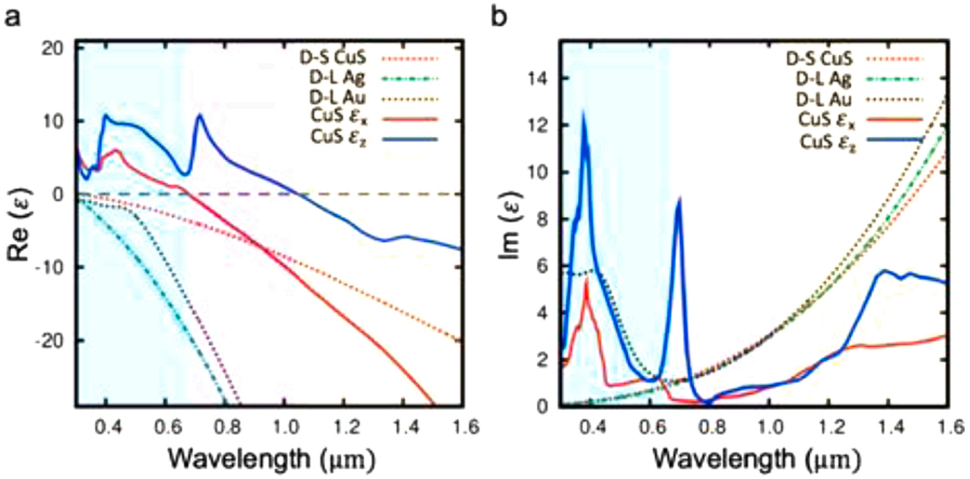

Fig. 11. Wavelength dependence of the real (a) and imaginary (b) parts of the calculated permittivity for different nanomaterials and computation methods. D-S indicates that the Drude-Sommerfeld method was employed in the calculation of CuS nanoparticles for comparison. D-L indicates the Drude-Lorentz model was used for both noble metals. Two spatial components (ε_x and ε_z) are displayed for the permittivity computed according to a Green's function-based method. Adapted from Ref. [148] with permission. Copyright 2019 American Chemical Society.

Table 3
Properties of selected CuS PNPs.

Material	Coating agent	Size, LSPR maximum	Q_A / Q_E (method)	Observed ΔT, macroscopic PCE (η) according to Eq. (4)	Excitation wavelength, irradiation conditions	Reference
CuS nanodisks	PEG	$d = 11$ nm 930 nm		55 K	808 nm, cw 16 W / cm^2 300 s	[151]
Flower-like CuS PNPs	PVP	$d \sim 1$ μm > 1080 nm		20.7 K	980 nm, cw 0.51 W / cm^2 300 s	[155]
Cu_9S_5 platelets	Amino-caproic acid	$d = 70$ nm $h = 13$ nm > 1100 nm		15.1 K η = 0.257	980 nm, cw 0.51 W / cm^2 600 s	[125]
$Cu_{7,2}S_4$ spheroids	Oleyl-amine / oleic acid	$d = 20$ nm 978 nm		19.5 K η = 0.567	980 nm, cw 0.72 W / cm^2 420 s	[156]
CuS nano-bundles	PVP / thioacetate	~ 3 μm length > 1100 nm		32 K η = 0.726	980 nm, cw 1 W / cm^2 2000s	[157]
CuS spheroids	PMA	$d = 18$ nm 965 nm		20 K η = 0.419	980 nm, cw 1.5 W / cm^2 720 s	[154]
CuS nanorods	PEI	6.5 × 38.5 nm 1277 nm		35 K η = 0.366	1064 nm, 1.33 W / cm^2 600 s	[158]
Cu_9S_8 nanodots	PEI	$d = 6.5$ nm 1148 nm		43 K η = 0.490	1064 nm, cw 1.33 W / cm^2 600 s	[158]
CuS nanoflakes	Brij52 / Igepal CO-630	$d = 371 \pm 35$ nm 1300 nm	0.72 (PA method)		1064 nm, pulsed ~ 10 ns pulses, 10 Hz repetition rate < 70 μJ / cm^2	[160]
CuS nanodisks	PEG	$d = 24.4$ nm $h = 4.0$ nm 1356 nm	0.99 (calculated)	10.22 ± 0.03 K (including 5.76 ± 0.04 K from water) η = 0.93 ± 0.03	1280 nm, cw 152 mW 175 s	[150]
CuS spheroids	mPEG H_2O-dispersed	$d = 35.5$ nm 970 nm		6.2 ± 0.1 K η = 0.582 ± 0.031 3.6 ± 0.1 K η = 0.714 ± 0.058	970 nm, cw 10.5 W / cm^2 1200 s 806 nm, cw 10.5 W / cm^2 1200 s	[161]
CuS spheroids	mPEG D_2O-dispersed	$d = 35.5$ nm 970 nm		4.2 ± 0.2 K η = 0.702 ± 0.042 3.3 ± 0.1 K η = 0.677 ± 0.034	970 nm, cw 10.5 W / cm^2 1200 s 806 nm. cw 10.5 W / cm^2 1200 s	[161]
Au-decorated CuS nanoplates	PVP	$d \cong$ 70 nm ~ 1100 nm		25.6 K η = 0.365	1064 nm, cw 250 mW 600 s	[162]
Core-shell Au-Cu_7S_4 hetero-structured nanorods	PEG	84.2 ± 5.9 nm × 36.6 ± 4.9 nm 803 nm	0.81 (calculated)	32.1 K η = 0.620	808 nm, cw 0.9 W cm^{-2} t = 600 s	[163]
Dumbbell-like Au Cu_7S_4 hetero-structured nanorods	PEG	61.4 ± 5.6 nm × 20.6 ± 3.8 nm 809 nm	0.95 (calculated)	31.2 K η = 0.558	808 nm, cw 0.9 W cm^{-2} t = 600 s	[163]
Au-Cu_9S_5 hybrid spheroids	Mixed polymer	$d = 10$ nm (core) $d = 20$ nm (total) ~ 1100 nm		15.8 K η = 0.37	1064 nm, cw 0.7 W cm^{-2} t = 600 s	[164]

Abbreviations used in the table: PEG, polyethylenglycol; d = spheroid diameter; cw, continuous wave; PVP, polyvinylpyrrolidone; h = disk thickness; PMA, modified poly(maleic anhydride); PEI, polyethyleneimine; PA, photoacoustic; mPEG, methylated polyethylenglycol.

excitation [165]. Mixed sulfide and selenide PNPs can display very high LSPR tunability (1400–1600 nm) as an advantageous feature [166]. In addition, semiconductor-based materials have been successfully combined with metals. One of these materials is based on Au / copper selenide heterodimers, which have displayed both versatility and sensitivity: 25 μg / mL *in vivo* for 1064 nm excitation in rats [167]. More generally, there have been many attempts to tune the LSPR maximum wavelength in various chalcogenide-based materials, while increasing their efficiency [168–170]. For example, the PCE of chalcopyrite ($CuFeS_2$) nanocrystals was shown to be higher than that of pure copper sulfide PNPs, as it reached the notable value of 0.49 at 808 nm excitation [171]. WS_2 nanodots yielded a similar PCE value (0.443) at this wavelength [172]. Nowadays, new compounds are extending the opportunities found in metal and semiconductor nanomaterials. Ni_xMoO_3 nanodots, for example, display especially high PCE at 808 nm excitation, where many photoactive materials are tested [173].

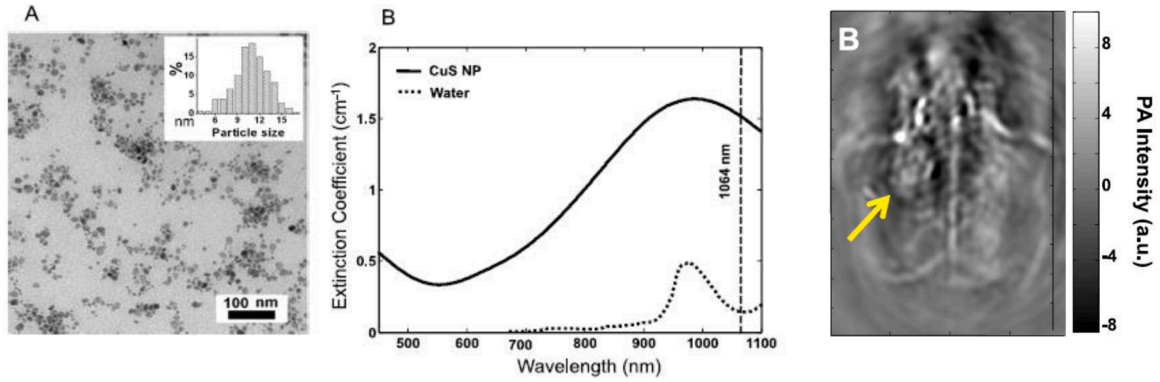

Fig. 12. (from left to right) TEM image of CuS PNPs. The diameter of the spheroids was 11 ± 3 nm (see inset). LSPR band of these PNPs dispersed in water. The extinction of pure water is displayed for comparison. The dashed line indicates the excitation wavelength for PAI. Image of a mouse brain where CuS PNPs were injected into a nodule. The image of the nodule is highlighted by an arrow. Adapted with permission from Ref. [152]. Copyright 2012 American Chemical Society.

8. Summary and perspectives

We have collected and contrasted a significant number of examples taken from various areas of the scientific literature. Altogether they show the growing importance of nanostructured inorganic materials in photoacoustics. Moreover, we have addressed an especially interesting aspect of this field, i.e., assessing the contribution that photoacoustics can give to the evaluation of favourable PNP properties. This consideration leads specifically to the question whether photoacoustic techniques can be employed for a quantitative measurement of the efficiency of the processes involved in photothermal conversion. An examination of both experimental and computational results strengthens the view that photoacoustic measurements yield accurate figures of optothermal properties (over a wide range of excitation wavelengths) due to their microscopic nature. In fact, the measurement of calibrated photoacoustic signals has been essential for the reliable determination of the Q_A / Q_E ratio. The importance of this quantity cannot be overrated, especially for medical applications of inorganic materials where the attainment of high photoconversion efficiency is particularly desirable. An early report of PNPs in 2003 reported the use of Au nanoshells with silica core in a study to verify whether photothermal therapy could be a viable approach for the treatment of solid tumours [174]. A temperature increase was observed for both isolated human cells and whole model animals upon irradiation at 820 nm. The application of photothermal therapy has built upon these and related findings to an impressively high degree. Recently, selective photoablation of prostata tumours has been performed for therapeutic purposes by the use of Au nanoshells in human patients. The evaluation of these results shows that the treatment is successful under many points of view, including patient safety [175].

Besides therapeutic applications, diagnostic tools based on photoacoustics are gaining popularity in biomedical areas. A pioneering study demonstrated the favourable contrast enhancement by Au PNPs in the *in vivo* photoacoustic tomography of a whole rat brain [176]. Increasingly complicated biological tissues can be now visualized according to their position and function by optoacoustic imaging techniques. Varying the excitation light wavelength is an opportunity which adds multidimensionality to photoacoustic investigations. It can be foreseen that more beneficial applications in biomedicine will soon become evident with the development of advanced plasmonic contrast agents, especially in the NIR range.

Declaration of Competing Interest

The authors declare that there are no conflicts of interest.

Acknowledgements

We wish to acknowledge all our collaborators in the field of nanoparticles photoacoustics, in particular Prof. P.R. Salvi, Prof. M. Becucci, Prof. C. Ferrante, Prof. R. Signorini and Prof. S. Gross. We thank Dr. B.D. Howes for carefully reading the manuscript. A.F. wishes to thank Prof. S. E. Braslavsky for her able guidance into laser-induced optoacoustic spectroscopy.

Our work was supported by the Italian Ministry for University and Research.

References

[1] Y. Liu, P. Bhattarai, Z. Dai, X. Chen, Photothermal therapy and photoacoustic imaging via nanotheranostics in fighting cancer, Chem. Soc. Rev. 48 (2019) 2053–2108, https://doi.org/10.1039/c8cs00618k.
[2] C. Moore, J.V. Jokerst, Strategies for image-guided therapy, surgery, and drug delivery using photoacoustic imaging, Theranostics 9 (2019) 1550–1571, https://doi.org/10.7150/thno.32362.
[3] Q. Fu, R. Zhu, J. Song, H. Yang, X. Chen, Photoacoustic imaging: contrast agents and their biomedical applications, Adv. Mater. 31 (2019) 1805875, https://doi.org/10.1002/adma.201805875.
[4] P.K. Jain, K.S. Lee, I.H. El-Sayed, M.A. El-Sayed, Calculated absorption and scattering properties of gold nanoparticles of different size, shape, and composition: applications in biological imaging and biomedicine, J. Phys. Chem. B 110 (2006) 7238–7248, https://doi.org/10.1021/jp057170o.
[5] W. Wei, X. Zhang, S. Zhang, G. Wei, Z. Su, Biocompatible and bioactive engineered nanomaterials for targeted tumor photothermal therapy: a review, Mater. Sci. Eng. C 104 (2019) 109891, https://doi.org/10.1016/j.msec.2019.109891.
[6] V. Ntziachristos, D. Razansky, Molecular imaging by means of multispectral optoacoustic tomography (MSOT), Chem. Rev. 110 (2010) 2783–2794, https://doi.org/10.1021/cr9002566.
[7] Y. Mantri, J.V. Jokerst, Engineering plasmonic nanoparticles for enhanced photoacoustic imaging, ACS Nano 14 (2020) 9408–9422, https://doi.org/10.1021/acsnano.0c05215.
[8] S. Mallidi, G.P. Luke, S. Emelianov, Photoacoustic imaging in cancer detection, diagnosis, and treatment guidance, Trends Biotechnol. 29 (2011) 213–221, https://doi.org/10.1016/j.tibtech.2011.01.006.
[9] L. Nie, X. Chen, Structural and functional photoacoustic molecular tomography aided by emerging contrast agents, Chem. Soc. Rev. 43 (2014) 7132–7170, https://doi.org/10.1039/c4cs00086b.
[10] X.L. Deán-Ben, S. Gottschalk, B. Mc Larney, S. Shoham, D. Razansky, Advanced optoacoustic methods for multiscale imaging of in vivo dynamics, Chem. Soc. Rev. 46 (2017) 2158–2198, https://doi.org/10.1039/c6cs00765a.
[11] C. Bohren, D. Huffman, Absorption and Scattering of Light By Small Particles, Wiley, New York, 1983.
[12] K.A. Willets, R.P. Van Duyne, Localized Surface Plasmon Resonance Spectroscopy and Sensing, Annu. Rev. Phys. Chem. 58 (2007) 267–297, https://doi.org/10.1146/annurev.physchem.58.032806.104607.
[13] E. Le Ru, P. Etchegoin, Principles of Surface-enhanced Raman Spectroscopy and Related Plasmonic Effects, Elsevier, Amsterdam, Oxford, 2008.
[14] V. Amendola, M. Meneghetti, Size evaluation of gold nanoparticles by UV–vis spectroscopy, J. Phys. Chem. C 113 (2009) 4277–4285, https://doi.org/10.1021/jp8082425.
[15] R. Yu, L.M. Liz-Marzán, F.J. García de Abajo, Universal analytical modeling of plasmonic nanoparticles, Chem. Soc. Rev. 46 (2017) 6710–6724, https://doi.org/10.1039/c6cs00919k.

[16] N. Li, P. Zhao, D. Astruc, Anisotropic gold nanoparticles: synthesis, properties, applications, and toxicity, Angew. Chem. Int. Ed. 53 (2014) 1756–1789, https://doi.org/10.1002/anie.201300441.

[17] Y. Lyu, J. Li, K. Pu, Second near-infrared absorbing agents for photoacoustic imaging and photothermal therapy, Small Methods 3 (2019) 1900553, https://doi.org/10.1002/smtd.201900553.

[18] M. Xu, L.V. Wang, Photoacoustic imaging in biomedicine, Rev. Sci. Instrum. 77 (2006), 041101, https://doi.org/10.1063/1.2195024.

[19] L.V. Wang, S. Hu, Photoacoustic Tomography: In Vivo Imaging from Organelles to Organs, Science 335 (2012) 1458–1462, https://doi.org/10.1126/science.1216210.

[20] J. Yao, L.V. Wang, Sensitivity of photoacoustic microscopy, Photoacoustics 2 (2014) 87–101, doi: 10./j.pacs.2014.04.002.

[21] A.B.E. Attia, G. Balasundaram, M. Moothanchery, U.S. Dinish, R. Bi, V. Ntziachristos, M. Olivo, A review of clinical photoacoustic imaging: current and future trends, Photoacoustics 16 (2019) 100144, https://doi.org/10.1016/j.pacs.2019.100144.

[22] C. Moore, F. Chen, J. Wang, J.V. Jokerst, Listening for the therapeutic window: advances in drug delivery utilizing photoacoustic imaging, Adv. Drug Deliv. Rev. 144 (2019) 78–89, https://doi.org/10.1016/j.addr.2019.07.003.

[23] E.C. Dreaden, A.M. Alkilany, X. Huang, C.J. Murphy, M.A. El-Sayed, The golden age: gold nanoparticles for biomedicine, Chem. Soc. Rev. 41 (2012) 2740–2779, https://doi.org/10.1039/c1cs15237h.

[24] A. Karlas, N.-A. Fasoula, K. Paul-Yuan, J. Reber, M. Kallmayer, D. Bozhko, M. Seeger, H.-H. Eckstein, M. Wildgruber, V. Ntziachristos, Cardiovascular optoacoustics: from mice to men – a review, Photoacoustics 14 (2019) 19–30, https://doi.org/10.1016/j.pacs.2019.03.001.

[25] I. Steinberg, D.M. Huland, O. Vermesh, H.E. Frostig, W.S. Tummers, S. S. Gambhir, Photoacoustic clinical imaging, Photoacoustics 14 (2019) 77–98, https://doi.org/10.1016/j.pacs.2019.05.001.

[26] M. Bouché, J.C. Hsu, Y.C. Dong, J. Kim, K. Taing, D.P. Cormode, Recent advances in molecular imaging with gold nanoparticles, Bioconjugate Chem. 31 (2020) 303–314, https://doi.org/10.1021/acs.bioconjchem.9b00669.

[27] T.A. Tabish, P. Dey, S. Mosca, M. Salimi, F. Palombo, P. Matousek, N. Stone, Smart gold nanostructures for light mediated Cancer theranostics: combining optical diagnostics with photothermal therapy, Adv. Sci. (2020) 1903441, https://doi.org/10.1002/advs.201903441.

[28] M.P. Melancon, M. Zhou, C. Li, Cancer Theranostics with Near-Infrared Light-Activatable Multimodal Nanoparticles, Acc. Chem. Res. 44 (2011) 947–956, https://doi.org/10.1021/ar200022e.

[29] M. Ha, J.-H. Kim, M. You, Q. Li, C. Fan, J.-M. Nam, Multicomponent plasmonic nanoparticles: from heterostructured nanoparticles to colloidal composite nanostructures, Chem. Rev. 119 (2019) 12208–12278, https://doi.org/10.1021/acs.chemrev.9b00234.

[30] J.E. Lemaster, J.V. Jokerst, What is new in nanoparticle-based photoacoustic imaging?, WIREs Nanomed, Nanobiotechnol. 9 (2017) e1404, https://doi.org/10.1002/wnan.1404.

[31] U. Kreibig, M. Vollmer, Optical Properties of Metal Clusters, Springer, Berlin, Heidelberg, New York, 1995.

[32] K.-S.- Lee, M.A. El-Sayed, Gold and silver nanoparticles in sensing and imaging: sensitivity of plasmon response to size, shape, and metal composition, J. Phys. Chem. B 110 (2006) 19220–19225, https://doi.org/10.1021/jp062536y.

[33] G. Frens, Controlled nucleation for the regulation of the particle size in monodisperse gold dispersions, Nature: Phys. Sci. 241 (1973) 20–22, https://doi.org/10.1038/physci241020a0.

[34] D.D. Evanoff Jr., G. Chumanov, Size-Controlled Synthesis of Nanoparticles. 2. Measurement of Extinction, Scattering, and Absorption Cross Sections, J. Phys. Chem. B 108 (2004) 13957–13962, https://doi.org/10.1021/jp0475640.

[35] B. Nikoobakht, M.A. El-Sayed, Preparation and growth mechanism of gold nanorods (NRs) using seed-mediated growth method, Chem. Mater. 15 (2003) 1957–1962, https://doi.org/10.1021/cm020732l.

[36] J.R. Cole, N.A. Mirin, M.W. Knight, G.P. Goodrich, N.J. Halas, Photothermal efficiencies of nanoshells and nanorods for clinical therapeutic applications, J. Phys. Chem. C 113 (2009) 12090–12094, https://doi.org/10.1021/jp9003592.

[37] X. Huang, P.K. Jain, I.H. El-Sayed, M.A. El-Sayed, Plasmonic photothermal therapy (PPTT) using gold nanoparticles, Lasers Med. Sci. 23 (2008) 217–228, https://doi.org/10.1007/s10103-007-0470-x.

[38] X. Huang, S. Neretina, M.A. El-Sayed, Gold Nanorods: From Synthesis and Properties to Biological and Biomedical Applications, Adv. Mater. 21 (2009) 4880–4910, https://doi.org/10.1002/adma.200802789.

[39] H.-H. Chang, C.J. Murphy, Mini gold nanorods with tunable plasmonic peaks beyond 1000 nm, Chem. Mater. 30 (2018) 1427–1435, https://doi.org/10.1021/acs.chemmater.7b05310.

[40] R. Takahata, S. Yamazoe, K. Koyasu, K. Imura, T. Tsukuda, Gold ultrathin nanorods with controlled aspect ratios and surface modifications: formation mechanism and localized surface plasmon resonance, J. Am. Chem. Soc. 140 (2018) 6640–6647, https://doi.org/10.1021/jacs.8b02884.

[41] L. Cavigli, S. Centi, C. Borri, P. Tortoli, I. Panettieri, I. Streit, D. Ciofini, G. Magni, F. Rossi, S. Siano, F. Ratto, R. Pini, 1064-nm-resonant gold nanorods for photoacoustic theranostics within permissible exposure limits, J. Biophotonics (2019) e201900082, https://doi.org/10.1002/jbio.201900082.

[42] K. Cheng, S.-R. Kothapalli, H. Liu, A.L. Koh, J.V. Jokerst, H. Jiang, M. Yang, J. Li, J. Levi, J.C. Wu, S.S. Gambhir, Z. Cheng, Construction and validation of nano gold tripods for molecular imaging of living subjects, J. Am. Chem. Soc. 136 (2014) 3560–3571, https://doi.org/10.1021/ja412001e.

[43] A. Guerrero-Martínez, S. Barbosa, I. Pastoriza-Santos, L.M. Liz-Marzán, Nanostars shine bright for you: colloidal synthesis, properties and applications of branched metallic nanoparticles, Curr. Opin. Coll. Interf. Sci. 16 (2011) 118–127, https://doi.org/10.1016/j.cocis.2010.12.007.

[44] C.G. Khoury, T. Vo-Dinh, Gold nanostars for surface-enhanced raman scattering: synthesis, characterization and optimization, J. Phys. Chem. C 112 (2008) 18849–18859, https://doi.org/10.1021/jp8054747.

[45] H. Wang, D.W. Brandl, P. Nordlander, N.J. Halas, Plasmonic nanostructures: artificial molecules, Acc. Chem. Res. 40 (2007) 53–62, https://doi.org/10.1021/ar0401045.

[46] A. Lalisse, G. Tessier, J. Plain, G. Baffou, Quantifying the efficiency of plasmonic materials for near-field enhancement and photothermal conversion, J. Phys. Chem. C 119 (2015) 25518–25528, https://doi.org/10.1021/acs.jpcc.5b09294.

[47] M. Rycenga, C.M. Cobley, J. Zeng, W. Li, C.H. Moran, Q. Zhang, D. Qin, Y. Xia, Controlling the synthesis and assembly of silver nanostructures for plasmonic applications, Chem. Rev. 111 (2011) 3669–3712, https://doi.org/10.1021/cr100275d.

[48] V. Amendola, R. Pilot, M. Frasconi, O.M. Maragò, M.A. Iatì, Surface plasmon resonance in gold nanoparticles: a review, J. Phys. Condens. Matter 29 (2017) 203002, https://doi.org/10.1088/1361-648X/aa60f3.

[49] A. Comin, L. Manna, New materials for tunable plasmonic colloidal nanocrystals, Chem. Soc. Rev. 43 (2014) 3957–3975, https://doi.org/10.1039/c3cs60265f.

[50] B. Doiron, M. Mota, M.P. Wells, R. Bower, A. Mihai, Y. Li, L.F. Cohen, N.Mc N. Alford, P.K. Petrov, R.F. Oulton, S.A. Maier, Quantifying figures of merit for localized surface plasmon resonance applications: a materials survey, ACS Photonics 6 (2019) 240–259, https://doi.org/10.1021/acsphotonics.8b01369.

[51] S.E. Braslavsky, Glossary of terms used in photochemistry 3rd edition (IUPAC recommendations 2006), Pure Appl. Chem. 79 (2007) 293–465, https://doi.org/10.1351/pac200779030293.

[52] R. García-Álvarez, L. Chen, A. Nedilko, A. Sánchez-Iglesias, A. Rix, Wi. Lederle, V. Pathak, T. Lammers, G. von Plessen, K. Kostarelos, L.M. Liz-Marzán, A.J. C. Kuehne, D.N. Chigrin, Optimizing the geometry of photoacoustically active gold nanoparticles for biomedical imaging, ACS Photonics 7 (2020) 646–652, https://doi.org/10.1021/acsphotonics.9b01418.

[53] S.E. Braslavsky, G.E. Heibel, Time-resolved photothermal and photoacoustic methods applied to photoinduced processes in solution, Chem. Rev. 92 (1992) 1381–1410, https://doi.org/10.1021/cr00014a007.

[54] G. Baffou, R. Quidant, Thermo-plasmonics: using metallic nanostructures as nano-sources of heat, Laser Photonics Rev. 7 (2013) 171–187, https://doi.org/10.1002/lpor.201200003.

[55] C.K.N. Patel, A.C. Tam, Pulsed optoacoustic spectroscopy of condensed matter, Rev. Mod. Phys. 53 (1981) 517–550, https://doi.org/10.1103/RevModPhys.53.517.

[56] A.C. Tam, Applications of photoacoustic sensing techniques, Rev. Mod. Phys. 58 (1986) 381–431, https://doi.org/10.1103/RevModPhys.58.381.

[57] J. Rudzki Small, N.S. Foster, J.E. Amonette, T. Autrey, Listening to colloidal silica samples: simultaneous measurement of absorbed and scattered light using pulsed-laser photoacoustics, Appl. Spectrosc. 54 (2000) 1142–1150, https://doi.org/10.1366/0003702001950940.

[58] Y.-S. Chen, W. Frey, S. Aglyamov, S. Emelianov, Environment-dependent generation of photoacoustic waves from plasmonic nanoparticles, Small 8 (2012) 47–52, https://doi.org/10.1002/smll.201101140.

[59] A. Feis, C. Gellini, P.R. Salvi, M. Becucci, Photoacoustic excitation profiles of gold nanoparticles, Photoacoustics 2 (2014) 47–53, https://doi.org/10.1016/j.pacs.2013.12.001.

[60] G.A. Pang, J. Laufer, R. Niessner, C. Haisch, Photoacoustic signal generation in gold nanospheres in aqueous solution: signal generation enhancement and particle diameter effects, J. Phys. Chem. C 120 (2016) 27646–27656, https://doi.org/10.1021/acs.jpcc.6b09374.

[61] R. Gao, Z. Xu, Y. Ren, L. Song, C. Liu, Nonlinear mechanisms in photoacoustics—powerful tools in photoacoustic imaging, Photoacoustics 22 (2021) 100243, https://doi.org/10.1016/j.pacs.2021.100243.

[62] A. Hatef, S. Fortin-Deschênes, E. Boulais, F. Lesage, M. Meunier, Photothermal response of hollow gold nanoshell to laser irradiation: continuous wave, short and ultrashort pulse, Int. J. Heat Mass Transf. 89 (2015) 866–871, https://doi.org/10.1016/j.ijheatmasstransfer.2015.05.071.

[63] K. Shahbazi, W. Frey, Y.-S. Chen, S. Aglyamov, S. Emelianov, Photoacoustics of core–shell nanospheres using comprehensive modeling and analytical solution approach, Commun. Phys. 2 (2019) 119, https://doi.org/10.1038/s42005-019-0216-7.

[64] D. Kumar, D.P. Ghai, R.K. Soni, Simulation studies of photoacoustic response from Gold-Silica core-shell nanoparticles, Plasmonics 13 (2018) 1833–1841, https://doi.org/10.1007/s11468-018-0697-3.

[65] A. Prost, F. Poisson, E. Bossy, Photoacoustic generation by a gold nanosphere: from linear to nonlinear thermoelastics in the long-pulse illumination regime, Phys. Rev. B 92 (2015) 115450, https://doi.org/10.1103/PhysRevB.92.115450.

[66] K. Metwally, S. Mensah, G. Baffou, Fluence threshold for photothermal bubble generation using plasmonic nanoparticles, J. Phys. Chem. C 119 (2015) 28586–28596, https://doi.org/10.1021/acs.jpcc.5b09903.

[67] S.V. Egerev, A.A. Oraevsky, Optothermoacoustic phenomena in highly diluted suspensions of gold nanoparticles, Int. J. Thermophys. 29 (2008) 2116–2125, https://doi.org/10.1007/s10765-008-0541-7.

[68] O. Simandoux, A. Prost, J. Gateau, E. Bossy, Influence of nanoscale temperature rises on photoacoustic generation: discrimination between optical absorbers based on thermal nonlinearity at high frequency, Photoacoustics 3 (2015) 20–25, https://doi.org/10.1016/j.pacs.2014.12.002.

[69] J.E. Alba-Rosales, G. Ramos-Ortiz, L.F. Escamilla-Herrera, B. Reyes-Ramírez, L. Polo-Parada, G. Gutiérrez-Juárez, Effects of optical attenuation, heat diffusion, and acoustic coherence in photoacoustic signals produced by nanoparticles, Appl. Phys. Lett. 112 (2018) 143101, https://doi.org/10.1063/1.5008873.
[70] G.A. Pang, C. Haisch, J. Laufer, Quenching of nonlinear photoacoustic signal generation in gold nanoparticles through coating, Nanoscale Adv. 2 (2020) 2699–2704, https://doi.org/10.1039/d0na00205d.
[71] J. Chen, B. Wiley, Z.-Y. Li, D. Campbell, F. Saeki, H. Cang, L. Au, J. Lee, X. Li, Y. Xia, Gold Nanocages, Engineering their structure for biomedical applications, Adv. Mater. 17 (2005) 2255–2261, https://doi.org/10.1002/adma.200500833.
[72] C. Kim, C. Favazza, L.V. Wang, In vivo photoacoustic tomography of chemicals: high-resolution functional and molecular optical imaging at New Depths, Chem. Rev. 110 (2010) 2756–2782, https://doi.org/10.1021/cr900266s.
[73] C. Kim, E.C. Cho, J. Chen, K.H. Song, L. Au, C. Favazza, Q. Zhang, C.M. Cobley, F. Gao, Y. Xia, L.V. Wang, In vivo molecular photoacoustic tomography of melanomas targeted by Bioconjugated gold nanocages, ACS Nano 4 (2010) 4559–4564, https://doi.org/10.1021/nn100736c.
[74] J.-S. Wi, J. Park, H. Kang, D. Jung, S.-W. Lee, T.G. Lee, Stacked gold nanodisks for bimodal photoacoustic and optical coherence imaging, ACS Nano 11 (2017) 6225–6232, https://doi.org/10.1021/acsnano.7b02337.
[75] J. Broda, G. Schmid, U. Simon, Size- and ligand-specific bioresponse of Gold clusters and nanoparticles: challenges and perspectives, in: D. Michael, P. Mingos (Eds.), Gold Clusters, Colloids and Nanoparticles I, Structure and Bonding Book Series (STRUCTURE, Volume 161), Springer International Publishing, Switzerland, 2013, pp. 189–242, https://doi.org/10.1007/430_2013_127.
[76] X.Y. Wong, A. Sena-Torralba, R. Álvarez-Diduk, K. Muthoosamy, A. Merkoçi, Nanomaterials for nanotheranostics: tuning their properties according to disease needs, ACS Nano 14 (2020) 2585–2627, https://doi.org/10.1021/acsnano.9b08133.
[77] K.A. Willets, R.P. Van Duyne, Localized surface plasmon resonance spectroscopy and sensing, Annu. Rev. Phys. Chem. 58 (2007) 267–297, https://doi.org/10.1146/annurev.physchem.58.032806.104607.
[78] G. Chen, I. Roy, C. Yang, P.N. Prasad, Nanochemistry and nanomedicine for nanoparticle-based diagnostics and therapy, Chem. Rev. 116 (2016) 2826–2885, https://doi.org/10.1021/acs.chemrev.5b00148.
[79] A. Heuer-Jungemann, N. Feliu, I. Bakaimi, M. Hamaly, A. Alkilany, I. Chakraborty, A. Masood, M.F. Casula, A. Kostopoulou, E. Oh, K. Susumu, M. H. Stewart, I.L. Medintz, E. Stratakis, W.J. Parak, A.G. Kanaras, The role of Ligands in the chemical synthesis and applications of inorganic nanoparticles, Chem. Rev. 119 (2019) 4819–4880, https://doi.org/10.1021/acs.chemrev.8b00733.
[80] C. Vilches, R. Quidant, Targeted hyperthermia with plasmonic nanoparticles, in: W.J. Parak, N. Feliu (Eds.), Colloids for Nanobiotechnology: Synthesis, Characterization and Potential Applications, Frontiers of Nanoscience, Volume 16, Elsevier, The Netherlands, 2020, pp. 307–352, https://doi.org/10.1016/B978-0-08-102828-5.00012-7.
[81] P.K. Jain, K. Manthiram, J.H. Engel, S.L. White, J.A. Faucheaux, A.P. Alivisatos, Doped nanocrystals as plasmonic probes of redox chemistry, Angew. Chem. Int. Ed. 52 (2013) 13671–13675, https://doi.org/10.1002/anie.201303707.
[82] N. Jiang, X. Zhuo, J. Wang, Active plasmonics: principles, structures, and applications, Chem. Rev. 118 (2018) 3054–3099, https://doi.org/10.1021/acs.chemrev.7b00252.
[83] A.J. Mieszawska, W.J.M. Mulder, Z.A. Fayad, D.P. Cormode, Multifunctional gold nanoparticles for diagnosis and therapy of disease, J. Mol. Pharm. Org. Process Res. 10 (2013) 831–847, https://doi.org/10.1021/mp3005885.
[84] P.-C. Li, C.-R.C. Wang, D.-B. Shieh, C.-W. Wei, C.-K. Liao, C. Poe, S. Jhan, A.-A. Ding, Y.-N. Wu, In vivo photoacoustic molecular imaging with simultaneous multiple selective targeting using antibody-conjugated gold nanorods, Opt. Express 16 (2008) 18605–18615, https://doi.org/10.1364/OE.16.018605.
[85] G.A. Pang, F. Poisson, J. Laufer, C. Haisch, E. Bossy, Theoretical and experimental study of photoacoustic excitation of silica-coated gold nanospheres in water, J. Phys. Chem. C 124 (2020) 1088–1098, https://doi.org/10.1021/acs.jpcc.9b09040.
[86] W.-S. Chang, B. Willingham, L.S. Slaughter, S. Dominguez-Medina, P. Swanglap, S. Link, Radiative and nonradiative properties of single plasmonic nanoparticles and their assemblies, Acc. Chem. Res. 45 (2012) 1936–1945, https://doi.org/10.1021/ar200337u.
[87] W.-S. Chang, B.A. Willingham, L.S. Slaughter, B.P. Khanal, L. Vigderman, E. R. Zubarev, S. Link, Low absorption losses of strongly coupled surface plasmons in nanoparticle assemblies, Proc. Natl. Acad. Sci. U. S. A. 108 (2011) 19879–19884, https://doi.org/10.1073/pnas.1113563108.
[88] P. Nordlander, C. Oubre, E. Prodan, K. Li, M.I. Stockman, Plasmon hybridization in nanoparticle dimers, Nano Lett. 4 (2004) 899–903, https://doi.org/10.1021/nl049681c.
[89] L. Jauffred, A. Samadi, H. Klingberg, P.M. Bendix, L.B. Oddershede, Plasmonic heating of nanostructures, Chem. Rev. 119 (2019) 8087–8130, https://doi.org/10.1021/acs.chemrev.8b00738.
[90] N.J. Halas, S. Lal, W.-S. Chang, S. Link, P. Nordlander, Plasmons in strongly coupled metallic nanostructures, Chem. Rev. 111 (2011) 3913–3961, https://doi.org/10.1021/cr200061k.
[91] N. Zohar, L. Chuntonov, G. Haran, The simplest plasmonic molecules: metal nanoparticle dimers and trimers, J. Photochem. Photobiol. C Photochem. Rev. 21 (2014) 26–39, https://doi.org/10.1016/j.jphotochemrev.2014.10.002.
[92] D. Manchon, J. Lermé, T. Zhang, A. Mosset, C. Jamois, C. Bonnet, J.-M. Rye, A. Belarouci, M. Broyer, M. Pellarina, E. Cottancin, Plasmonic coupling with most of the transition metals: a new family of broad band and near infrared nanoantennas, Nanoscale 7 (2015) 1181–1192, https://doi.org/10.1039/c4nr05383d.
[93] J.H. Yoon, F. Selbach, L. Schumacher, J. Jose, S. Schlücker, Surface plasmon coupling in dimers of gold nanoparticles: experiment and theory for ideal (Spherical) and nonideal (Faceted) building blocks, ACS Photonics 6 (2019) 642–648, https://doi.org/10.1021/acsphotonics.8b01424.
[94] Q.-H. Wei, K.-H. Su, S. Durant, X. Zhang, Plasmon resonance of finite one-dimensional Au nanoparticle chains, Nano Lett. 4 (2004) 1067–1071, https://doi.org/10.1021/nl049604h200.4.6.
[95] M. Lin, C. Guo, J. Li, D. Zhou, K. Liu, X. Zhang, T. Xu, H. Zhang, L. Wang, B. Yang, Polypyrrole-coated chainlike gold nanoparticle architectures with the 808 nm photothermal transduction efficiency up to 70%, ACS Appl. Mater. Interfaces 6 (2014) 5860–5868, https://doi.org/10.1021/am500715f.
[96] L. Khosravi Khorashad, L.V. Besteiro, Z. Wang, J. Valentine, A.O. Govorov, Localization of Excess Temperature Using Plasmonic Hot Spots in Metal Nanostructures: Combining Nano-Optical Antennas with the Fano Effect, J. Phys. Chem. C 120 (2016) 13215–13226, https://doi.org/10.1021/acs.jpcc.6b03644.
[97] M. Yorulmaz, A. Hoggard, H. Zhao, F. Wen, W.-S. Chang, N.J. Halas, P. Nordlander, S. Link, Absorption spectroscopy of an individual Fano cluster, Nano Lett. 16 (2016) 6497–6503, https://doi.org/10.1021/acs.nanolett.6b03080.
[98] A. Joplin, W.-S. Chang, S. Link, Imaging and spectroscopy of single metal nanostructure absorption, Langmuir 34 (2018) 3775–3786, https://doi.org/10.1021/acs.langmuir.7b03154.
[99] S. Mallidi, S. Kim, A. Karpiouk, P.P. Joshi, K. Sokolov, S. Emelianov, Visualization of molecular composition and functionality of cancer cells using nanoparticle-augmented ultrasound-guided photoacoustics, Photoacoustics 3 (2015) 26–34, https://doi.org/10.1016/j.pacs.2014.12.003.
[100] C.L. Bayer, S.Y. Nam, Y.-S. Chen, S.Y. Emelianov, Photoacoustic signal amplification through plasmonic nanoparticle aggregation, J. Biomed. Opt. 18 (2013), 016001, https://doi.org/10.1117/1.JBO.
[101] I.-C. Sun, C.-H. Ahn, K. Kim, S. Emelianov, Photoacoustic imaging of cancer cells with glycol-chitosan-coated gold nanoparticles as contrast agents, J. Biomed. Opt. 24 (2019) 121903, https://doi.org/10.1117/1.JBO.24.12.121903.
[102] E. Boulais, R. Lachaine, A. Hatef, M. Meunier, Plasmonics for pulsed-laser cell nanosurgery: fundamentals and applications, J. Photochem. Photobiol. C Photochem. Rev. 17 (2013) 26–49, https://doi.org/10.1016/j.jphotochemrev.2013.06.001.
[103] D. Jaque, L. Martínez Maestro, B. del Rosal, P. Haro-Gonzalez, A. Benayas, J. L. Plaza, E. Martín Rodríguez, J. García Solé, Nanoparticles for photothermal therapies, Nanoscale 6 (2014) 9494–9530, https://doi.org/10.1039/c4nr00708e.
[104] L. Cheng, C. Wang, L. Feng, K. Yang, Z. Liu, Functional nanomaterials for phototherapies of cancer, Chem. Rev. 114 (2014) 10869–10939, https://doi.org/10.1021/cr400532z.
[105] R.S. Riley, E.S. Day, Gold nanoparticle-mediated photothermal therapy: applications and opportunities for multimodal cancer treatment, WIREs Nanomed. Nanobiotechnol. 9 (2017) e1449, https://doi.org/10.1002/wnan.1449.
[106] S.K. Sharma, N. Shrivastava, F. Rossi, L.D. Tung, N.T.K. Thanh, Nanoparticles-based magnetic and photo induced hyperthermia for cancer treatment, Nano Today 29 (2019), 100795, https://doi.org/10.1016/j.nantod.2019.100795.
[107] M.R.K. Ali, Y. Wu, M.A. El-Sayed, Gold-nanoparticle-Assisted plasmonic photothermal therapy advances toward clinical application, J. Phys. Chem. C 123 (2019) 15375–15393, https://doi.org/10.1021/acs.jpcc.9b01961.
[108] W. Lu, M.P. Melancon, C. Xiong, Q. Huang, A. Elliott, S. Song, R. Zhang, L. G. Flores, J.G. Gelovani, L.V. Wang, G. Ku, R.J. Stafford, C. Li, Effects of photoacoustic imaging and photothermal ablation therapy mediated by targeted hollow gold nanospheres in an orthotopic mouse xenograft model of glioma, Cancer Res. 71 (2011) 6116–6121, https://doi.org/10.1158/0008-5472.CAN-10-4557.
[109] T.L. Doane, C. Burda, The unique role of nanoparticles in nanomedicine: imaging, drug delivery and therapy, Chem. Soc. Rev. 41 (2012) 2885–2911, https://doi.org/10.1039/c2cs15260f.
[110] H.S. Kim, D.Y. Lee, Photothermal therapy with gold nanoparticles as an anticancer medication, J. Pharm. Investig. 47 (2017) 19–26, https://doi.org/10.1007/s40005-016-0292-6.
[111] Y.-S. Chen, W. Frey, C. Walker, S. Aglyamov, S. Emelianov, Sensitivity enhanced nanothermal sensors for photoacoustic temperature mapping, J. Biophotonics 6 (2013) 534–542, https://doi.org/10.1002/jbio.201200219.
[112] N.S. Abadeer, C.J. Murphy, Recent progress in Cancer Thermal therapy using gold nanoparticles, J. Phys. Chem. C 120 (2016) 4691–4716, https://doi.org/10.1021/acs.jpcc.5b11232.
[113] C. Bi, J. Chen, Y. Chen, Y. Song, A. Li, S. Li, Z. Mao, C. Gao, D. Wang, H. Möhwald, H. Xia, Realizing a Record Photothermal Conversion Efficiency of Spiky Gold Nanoparticles in the Second Near-Infrared Window by Structure Based Rational Design, Chem. Mater. 30 (2018) 2709–2718, https://doi.org/10.1021/acs.chemmater.8b00312.
[114] Y. Wang, K.C.L. Black, H. Luehmann, W. Li, et al., A comparison study of gold nanohexapods, nanorods, and nanocages for photothermal Cancer treatment, ACS Nano 7 (2013) 2068–2077, https://doi.org/10.1021/nn304332s.
[115] H. Chen, L. Shao, T. Ming, Z. Sun, C. Zhao, B. Yang, J. Wang, Understanding the photothermal conversion efficiency of gold nanocrystals, Small 6 (2010) 2272–2280, https://doi.org/10.1002/smll.201001109.
[116] D.K. Roper, W. Ahn, M. Hoepfner, Microscale heat transfer transduced by surface plasmon resonant gold nanoparticles, J. Phys. Chem. C 111 (2007) 3636–3641, https://doi.org/10.1021/jp064341w.

[117] S.A. Lindley, J.Z. Zhang, Bumpy hollow gold nanospheres for theranostic applications: effect of surface morphology on photothermal conversion efficiency, ACS Appl. Nano Mater. 2 (2019) 1072–1081, https://doi.org/10.1021/acsanm.8b0233.
[118] H.H. Richardson, M.T. Carlson, P.J. Tandler, P. Hernandez, A.O. Govorov, Experimental and theoretical studies of light-to-Heat conversion and collective heating effects in metal nanoparticle solutions, Nano Lett. 9 (2009) 1139–1146, https://doi.org/10.1021/nl8036905.
[119] Z. Qin, J.C. Bischof, Thermophysical and biological responses of gold nanoparticle laser heating, Chem. Soc. Rev. 41 (2012) 1191–1217, https://doi.org/10.1039/c1cs15184c.
[120] C. Boutopoulos, A. Hatef, M. Fortin-Deschenes, M. Meunier, Dynamic imaging of single gold nanoparticle in liquid irradiated by off-resonance femtosecond laser, Nanoscale 27 (2015) 11758–11765, https://doi.org/10.1039/c5nr02721g.
[121] G. Baffou, P. Berto, E. Bermudez Ureña, R. Quidant, S. Monneret, J. Polleux, H. Rigneault, Photoinduced heating of nanoparticle arrays, ACS Nano 7 (2013) 6478–6488, https://doi.org/10.1021/nn401924n.
[122] Y.-S. Chen, Y. Zhao, S.J. Yoon, S.S. Gambhir, S. Emelianov, Miniature gold nanorods for photoacoustic molecular imaging in the second near-infrared optical window, Nat. Nanotechnol. 14 (2019) 465–472, https://doi.org/10.1038/s41565-019-0392-3.
[123] V.K. Pustovalov, A.S. Smetannikov, V.P. Zharov, Photothermal and accompanied phenomena of selective nanophotothermolysis with gold nanoparticles and laser pulses, Laser Phys. Lett. 5 (2008) 775–792, https://doi.org/10.1002/lapl.200810072.
[124] K. Jiang, D.A. Smith, A. Pinchuk, Size-dependent photothermal conversion efficiencies of plasmonically heated gold nanoparticles, J. Phys. Chem. C 117 (2013) 27073–27080, https://doi.org/10.1021/jp409067h.
[125] Q. Tian, F. Jiang, R. Zou, Q. Liu, Z. Chen, M. Zhu, S. Yang, J. Wang, J. Wang, J. Hu, Hydrophilic Cu_9S_5 nanocrystals: a photothermal agent with a 25.7% heat conversion efficiency for photothermal ablation of cancer cells in vivo, ACS Nano 5 (2011) 9761–9771, https://doi.org/10.1021/nn203293t.
[126] C.M. Hessel, V.P. Pattani, M. Rasch, M.G. Panthani, B. Koo, J.W. Tunnell, B. A. Korge, Copper selenide nanocrystals for photothermal therapy, Nano Lett. 11 (2011) 2560–2566, https://doi.org/10.1021/nl201400z.
[127] E.C. Cho, C. Kim, F. Zhou, C.M. Cobley, K.H. Song, J. Chen, Z.-Y. Li, L.V. Wang, Y. Xia, Measuring the Optical Absorption Cross Sections of Au-Ag Nanocages and Au Nanorods by Photoacoustic Imaging, J. Phys. Chem. C 113 (2009) 9023–9028, https://doi.org/10.1021/jp903343p.
[128] L.M. Maestro, P. Haro-González, J.G. Coello, D. Jaque, Absorption efficiency of gold nanorods determined by quantum dot fluorescence thermometry, Appl. Phys. Lett. 100 (2012) 201110, https://doi.org/10.1063/1.471860.
[129] L.M. Maestro, P. Haro-González, A. Sánchez-Iglesias, L.M. Liz-Marzán, J. García Solé, D. Jaque, Quantum dot thermometry evaluation of geometry dependent heating efficiency in gold nanoparticles, Langmuir 30 (2014) 1650–1658, https://doi.org/10.1021/la403435v.
[130] Z. Qin, Y. Wang, J. Randrianalisoa, V. Raeesi, W.C.W. Chan, W. Lipiński, J. C. Bischof, Quantitative comparison of photothermal heat generation between gold nanospheres and nanorods, Sci. Rep. 6 (2016) 29836, https://doi.org/10.1038/srep29836.
[131] B. Storti, F. Elisei, S. Abbruzzetti, C. Viappiani, L. Latterini, One-pot synthesis of gold nanoshells with high photon-to-Heat conversion efficiency, J. Phys. Chem. C 113 (2009) 7516–7521, https://doi.org/10.1021/jp810544b.
[132] V. Weber, A. Feis, C. Gellini, R. Pilot, P.R. Salvi, R. Signorini, Far- and near-field properties of gold nanoshells studied by photoacoustic and surface-enhanced Raman spectroscopies, Phys. Chem. Chem. Phys. 17 (2015) 21190–21197, https://doi.org/10.1039/c4cp05054a.
[133] C. Ayala-Orozco, C. Urban, M.W. Knight, A.S. Urban, O. Neumann, S.W. Bishnoi, S. Mukherjee, A.M. Goodman, H. Charron, T. Mitchell, M. Shea, R. Roy, S. Nanda, R. Schiff, N.J. Halas, A. Joshi, Au nanomatryoshkas as efficient near-infrared photothermal transducers for Cancer treatment: benchmarking against nanoshells, ACS Nano 8 (2014) 6372–6381, https://doi.org/10.1021/nn501871d.
[134] R. Bardhan, S. Mukherjee, N.A. Mirin, S.D. Levit, P. Nordlander, N.J. Halas, Nanosphere-in-a-Nanoshell: a simple nanomatryushka, J. Phys. Chem. C 114 (2010) 7378–7383, https://doi.org/10.1021/jp9095387.
[135] P. Huang, P. Rong, J. Lin, W. Li, X. Yan, M.G. Zhang, L. Nie, G. Niu, J. Lu, W. Wang, X. Chen, Triphase interface synthesis of plasmonic gold bellflowers as near-infrared light mediated acoustic and thermal theranostics, J. Am. Chem. Soc. 136 (2014) 8307–8313, https://doi.org/10.1021/ja503115n.
[136] A. Plan Sangnier, A. Van de Walle, R. Aufaure, M. Fradet, L. Motte, E. Guénin, Y. Lalatonne, C. Wilhelm, Endosomal Confinement of Gold Nanospheres, Nanorods, and Nanoraspberries Governs Their Photothermal Identity and Is Beneficial for Cancer Cell Therapy, Adv. Biosys. 4 (2020) 1900284, https://doi.org/10.1002/adbi.201900284.
[137] N. Micali, F. Mallamace, M. Castriciano, A. Romeo, L. Monsù Scolaro, Separation of scattering and absorption contributions in UV/Visible spectra of resonant systems, Anal. Chem. 73 (2001) 4958–4963, https://doi.org/10.1021/ac010379n.
[138] B.-J. Liu, K.-Q. Lin, S. Hu, X. Wang, Z.-C. Lei, H.-X. Lin, B. Ren, Extraction of absorption and scattering contribution of metallic nanoparticles toward rational synthesis and application, Anal. Chem. 87 (2015) 1058–1065, https://doi.org/10.1021/ac503612b.
[139] Y.-H. Chien, K.K. Chan, T. Anderson, K.V. Kong, B.K. Ng, K.-T. Yong, Advanced near-infrared light-responsive nanomaterials as therapeutic platforms for Cancer therapy, Adv. Therap. 2 (2019) 1800090, https://doi.org/10.1002/adtp.201800090.
[140] A. Agrawal, S.H. Cho, O. Zandi, S. Ghosh, R.W. Johns, D.J. Milliron, Localized surface plasmon resonance in semiconductor nanocrystals, Chem. Rev. 118 (2018) 3121–3207, https://doi.org/10.1021/acs.chemrev.7b00613.
[141] P. Bergstrom Mann, I.J. McGregor, M. S.Bourke, S. Burkitt-Gray, M.-T. M. Fairclough, M. Hogarth, N. Thanou, M. Long, Green, An atom efficient, single-source precursor route to plasmonic CuS nanocrystals, Nanoscale Adv. 1 (2019) 522–526, https://doi.org/10.1039/c8na00325d.
[142] J.T. Buchman, N.V. Hudson-Smith, K.M. Landy, C.L. Haynes, Understanding nanoparticle toxicity mechanisms to inform redesign strategies to reduce environmental impact, Acc. Chem. Res. 52 (2019) 1632–1642, https://doi.org/10.1021/acs.accounts.9b00053.
[143] Y. Zhao, H. Pan, Y. Lou, X. Qiu, J. Zhu, C. Burda, Plasmonic Cu2-xS nanocrystals: optical and structural properties of copper-deficient copper(I) sulfides, J. Am. Chem. Soc. 131 (2009) 4253–4261, https://doi.org/10.1021/ja805655b.
[144] Y. Xie, A. Riedinger, M. Prato, A. Casu, A. Genovese, P. Guardia, S. Sottini, C. Sangregorio, K. Miszta, S. Ghosh, T. Pellegrino, L. Manna, Copper sulfide nanocrystals with tunable composition by reduction of covellite nanocrystals with Cu^+ ions, J. Am. Chem. Soc. 135 (2013) 17630–17637, https://doi.org/10.1021/ja409754v.
[145] M. Zhou, M. Tian, C. Li, Copper-based nanomaterials for Cancer imaging and therapy, Bioconjugate Chem. 27 (2016) 1188–1199, https://doi.org/10.1021/acs.bioconjchem.6b00156.
[146] J.M. Luther, P.K. Jain, T. Ewers, A.P. Alivisatos, Localized surface plasmon resonances arising from free carriers in doped quantum dots, Nat. Mater. 10 (2011) 361, https://doi.org/10.1038/nmat3004.
[147] W. Xu, H. Liu, D. Zhou, X. Chen, N. Ding, H. Song, H. Ågren, Localized surface plasmon resonances in self-doped copper chalcogenide binary nanocrystals and their emerging applications, Nano Today 33 (2020) 100892, https://doi.org/10.1016/j.nantod.2020.100892.
[148] R.M. Córdova-Castro, M. Casavola, M. van Schilfgaarde, A.V. Krasavin, M. A. Green, D. Richards, A.V. Zayats, Anisotropic plasmonic CuS nanocrystals as a natural electronic material with hyperbolic optical dispersion, ACS Nano 13 (2019) 6550–6560, https://doi.org/10.1021/acsnano.9b00282.
[149] C. Yan, Q. Tian, S. Yang, Recent advances in the rational design of copper chalcogenide to enhance the photothermal conversion efficiency for the photothermal ablation of cancer cells, RSC Adv. 7 (2017) 37887, https://doi.org/10.1039/c7ra05468h.
[150] R. Marin, J. Lifante, L.V. Besteiro, Z. Wang, A.O. Govorov, F. Rivero, F. Alfonso, F. Sanz-Rodríguez, D. Jaque, Plasmonic copper sulfide nanoparticles enable dark contrast in optical coherence tomography, Adv. Healthc. Mater. 9 (2020) 1901627, https://doi.org/10.1002/adhm.201901627.
[151] M. Zhou, R. Zhang, M.A. Huang, W. Lu, S.L. Song, M.P. Melancon, M. Tian, D. Liang, C. Li, A Chelator-Free Multifunctional [64Cu]CuS Nanoparticle Platform for Simultaneous Micro-PET/CT Imaging and Photothermal Ablation Therapy, J. Am. Chem. Soc. 132 (2010) 15351–15358, https://doi.org/10.1021/ja106855m.
[152] G. Ku, M. Zhou, S. Song, Q. Huang, J. Hazle, C. Li, Copper sulfide nanoparticles As a new class of photoacoustic contrast agent for deep tissue imaging at 1064 nm, ACS Nano 6 (2012) 7489–7496, https://doi.org/10.1021/nn302782y.
[153] J. Mou, C. Liu, P. Li, Y. Chen, H. Xu, C. Wei, L. Song, J. Shi, H. Chen, A facile synthesis of versatile Cu2xS nanoprobe for enhanced MRI and infrared thermal/photoacoustic multimodal imaging, Biomaterials 57 (2015) 12–21, https://doi.org/10.1016/j.biomaterials.2015.04.020.
[154] F. Lu, J. Wang, C. Tao, J.-J. Zhu, Highly monodisperse beta-cyclodextrin-covellite nanoparticles for efficient photothermal and chemotherapy, Nanoscale Horiz. 3 (2018) 538–544, https://doi.org/10.1039/c8nh00026c.
[155] Q. Tian, M. Tang, Y. Sun, R. Zou, Z. Chen, M. Zhu, S. Yang, J. Wang, J. Wang, J. Hu, Hydrophilic flower-like CuS superstructures as an efficient 980 nm laser-driven photothermal agent for ablation of Cancer cells, Adv. Mater. 23 (2011) 3542–3547, https://doi.org/10.1002/adma.201101295.
[156] B. Li, Q. Wang, R. Zou, X. Liu, K. Xu, W. Li, J. Hu, $Cu_{7.2}S_4$ Nanocrystals: A Novel Photothermal Agent with a 56.7% Photothermal Conversion Efficiency for Photothermal Therapy of Cancer Cells, Nanoscale 6 (2014) 3274–3282, https://doi.org/10.1039/c3nr06242b.
[157] X. Bu, D. Zhou, J. Li, X. Zhang, K. Zhang, H. Zhang, B. Yang, Copper sulfide self-assembly architectures with improved photothermal performance, Langmuir 30 (2014) 1416–1423, https://doi.org/10.1021/la404009d.
[158] Z. Xu, N. Rao, C.-Y. Tang, C.-H. Cheng, W.-C. Law, Aqueous phase synthesis of Cu2−xS nanostructures and their photothermal generation study, ACS Omega 4 (2019) 14655–14662, https://doi.org/10.1021/acsomega.9b02204.
[159] J. Wang, S. Hsu, N. Gonzalez-Pech, A. Jhunjhunwala, F. Chen, A. Hariri, V. Grassian, A. Tao, J.V. Jokerst, Copper sulfide nanodisks and nanoprisms for photoacoustic ovarian tumor imaging, Part. Part. Syst. Charact. 36 (2019) 1900171, https://doi.org/10.1002/ppsc.201900171.
[160] G. Morgese, P. Dolcet, A. Feis, C. Gellini, S. Gialanella, A. Speghini, D. Badocco, P. Pastore, M. Casarin, S. Gross, Room-Temperature Crystallization of CuS Nanostructures for Photothermal Applications through a Nanoreactor Approach, Eur. J. Inorg. Chem. (2017) 2745–2754, https://doi.org/10.1002/ejic.201601435.
[161] R. Marin, A. Skripka, L.V. Besteiro, A. Benayas, Z. Wang, A.O. Govorov, P. Canton, F. Vetrone, Highly efficient copper sulfide-based near-infrared photothermal agents: exploring the limits of macroscopic heat conversion, Small 14 (2018) 1803282, https://doi.org/10.1002/smll.201803282.

[162] Z. Wang, N. Yu, X. Li, W. Yu, S. Han, X. Ren, S. Yin, M. Li, Z. Chen, Galvanic exchange-induced growth of Au nanocrystals on CuS nanoplates for imaging guided photothermal ablation of tumors, Chem. Eng. J. 381 (2020) 122613, https://doi.org/10.1016/j.cej.2019.122613.
[163] C. Leng, X. Zhang, F. Xu, Y. Yuan, H. Pei, Z. Sun, L. Li, Z. Bao, Engineering gold nanorod–Copper sulfide heterostructures with enhanced photothermal conversion efficiency and photostability, Small 14 (2018) 1703077, https://doi.org/10.1002/smll.201703077.
[164] X. Ding, C.H. Liow, M. Zhang, R. Huang, C. Li, H. Shen, M. Liu, Y. Zou, N. Gao, Z. Zhang, Y. Li, Q. Wang, S. Li, J. Jiang, Surface Plasmon Resonance Enhanced Light Absorption and Photothermal Therapy in the Second Near-Infrared Window, J. Am. Chem. Soc. 136 (2014) 15684–15693, https://doi.org/10.1021/ja508641z.
[165] X. Liu, W.C. Law, M. Jeon, X. Wang, M. Liu, C. Kim, P.N. Prasad, M.T. Swihart, Cu2-x Se nanocrystals with localized surface plasmon resonance as sensitive contrast agents for in vivo photoacoustic imaging: demonstration of sentinel lymph node mapping, Adv. Healthc. Mater. 2 (2013) 952–957, https://doi.org/10.1002/adhm.201200388.
[166] X. Liu, X. Wang, M.T. Swihart, $Cu_{2-x}S_{1-y}Se_y$ alloy nanocrystals with broadly tunable near-infrared localized surface plasmon resonance, Chem. Mater. 25 (2013) 4402–4408, https://doi.org/10.1021/cm402848k.
[167] X. Liu, C. Lee, W.-C. Law, D. Zhu, M. Liu, M. Jeon, J. Kim, P.N. Prasad, C. Kim, M. T. Swihart, Au−Cu_{2-x}Se heterodimer nanoparticles with broad localized surface plasmon resonance as contrast agents for deep tissue imaging, Nano Lett. 13 (2013) 4333–4339, https://doi.org/10.1021/nl402124h.
[168] X. Liu, M.T. Swihart, Heavily-doped colloidal semiconductor and metal oxide nanocrystals: an emerging new class of plasmonic nanomaterials, Chem. Soc. Rev. 43 (2014) 3908–3920, https://doi.org/10.1039/c3cs60417a.
[169] T.M. Mattox, X. Ye, K. Manthiram, P.J. Schuck, A.P. Alivisatos, J.J. Urban, Chemical control of plasmons in metal chalcogenide and metal oxide nanostructures, Adv. Mater. 27 (2015) 5830–5837, https://doi.org/10.1002/adma.201502218.
[170] C. Coughlan, M. Ibáñez, O. Dobrozhan, A. Singh, A. Cabot, K.M. Ryan, Compound copper chalcogenide nanocrystals, Chem. Rev. 117 (2017) 5865–6109, https://doi.org/10.1021/acs.chemrev.6b00376.
[171] S. Ghosh, T. Avellini, A. Petrelli, I. Kriegel, R. Gaspari, G. Almeida, G. Bertoni, A. Cavalli, F. Scotognella, T. Pellegrino, L. Manna, Colloidal $CuFeS_2$ nanocrystals: intermediate Fe d-Band leads to high photothermal conversion efficiency, Chem. Mater. 28 (2016) 4848–4858, https://doi.org/10.1021/acs.chemmater.6b02192.
[172] Y. Yong, X. Cheng, T. Bao, M. Zu, L. Yan, W. Yin, C. Ge, D. Wang, Z. Gu, Y. Zhao, Tungsten sulfide quantum dots as multifunctional nanotheranostics for in vivo dual-modal image-guided Photothermal/Radiotherapy synergistic therapy, ACS Nano 9 (2015) 12451–12463, https://doi.org/10.1021/acsnano.5b05825.
[173] X. Wang, P. Yan, Q. Xu, H. Li, C. Guo, C. Liu, Fabrication of quasi-metallic Ni_xMoO_3 nanodots for enhanced plasmon resonance and photothermal conversion, Chem. Commun. 55 (2019) 9777–9780, https://doi.org/10.1039/c9cc03987b.
[174] L.R. Hirsch, R.J. Stafford, J.A. Bankson, S.R. Sershen, B. Rivera, R.E. Price, J. D. Hazle, N.J. Halas, J.L. West, Nanoshell-mediated near-infrared thermal therapy of tumors under magnetic resonance guidance, Proc. Natl. Acad. Sci. U. S. A. 100 (2003) 13549–13554, doi: 10.1073pnas.2232479100.
[175] A.R. Rastinehad, H. Anastos, E. Wajswol, J.S. Winoker, J.P. Sfakianos, S. K. Doppalapudi, M.R. Carrick, C.J. Knauer, B. Taouli, S.C. Lewis, A.K. Tewari, J. A. Schwartz, S.E. Canfield, A.K. George, J.L. West, N.J. Halas, Gold nanoshell-localized photothermal ablation of prostate tumors in a clinical pilot device study, Proc. Natl. Acad. Sci. U. S. A. 116 (2019) 18590–18596, https://doi.org/10.1073/pnas.1906929116.
[176] Y. Wang, X. Xie, X. Wang, G. Ku, K.L. Gill, D.P. O'Neal, G. Stoica, L.V. Wang, Photoacoustic tomography of a nanoshell contrast agent in the in vivo rat brain, Nano Lett. 4 (2004) 1689–1692, https://doi.org/10.1021/nl049126a.

Cristina Gellini graduated in Chemistry at the University of Florence in 1992 and received her PhD in Chemistry in 1996. In 1997 worked as von Humboldt fellow at the Max Planck Institut für Strahlenchemie in Mülheim an der Ruhr. In 1998 got a postdoc position at the Chemistry Department of the University of Florence where became researcher in 2000. Main scientific interests are focused on the optical characterization of SERS active surfaces, optoacoustic spectroscopy of nano-systems and fluorescence properties of probe-chromophores.

Prof. Alessandro Feis graduated at the University of Florence in 1985 and received his Ph.D. in Chemistry from the University of Padua in 1990. After working as a postdoctoral fellow at the University of Mainz and at the former Max-Planck-Institut for Radiation Chemistry in Muelheim/Ruhr, he joined the Department of Chemistry of the University of Florence in 1996. He spent a sabbatical year at the Institute for the Structure of Matter of the CSIC in Madrid in 2012. He visited the Faculty of Chemistry of the University of Duisburg-Essen in 2016 and 2017. His main interests are in Raman and optoacoustic spectroscopy.